Changes in the endoplasmic reticulum-mitochondria communication in dermal fibroblasts from early-stage bipolar disorder patients: Skin-brain axis as a new route to understand the pathophysiology of mental illness?

ANA CATARINA PEREIRA[1-4], ANA PATRÍCIA MARQUES[1,3,4], ROSA RESENDE[1,3,4], LAURA SERRANO-CUÑARRO[1,3], MARGARIDA CALDEIRA[1,3,4], TÂNIA FERNANDES[1-4], MARIANA BATISTA[3,5], ANTÓNIO MACEDO[2,3,6,7], JOANA BARBOSA DE MELO[2,3,8,9], NUNO MADEIRA[2,3,6,7], CLÁUDIA CAVADAS[1,3,10], MARIA TERESA CRUZ[1,3,10] and CLÁUDIA FRAGÃO PEREIRA[1-3]

[1]Center for Neuroscience and Cell Biology (CNC-UC), Center for Innovative Biomedicine and Biotechnology (CiBB), University of Coimbra, 3004-504 Coimbra, Portugal; [2]Faculty of Medicine, University of Coimbra, 3000-370 Coimbra, Portugal; [3]Clinical and Academic Center of Coimbra (CACC), 3004-561 Coimbra, Portugal; [4]Institute for Interdisciplinary Research (IIIUC), University of Coimbra, 3030-789 Coimbra, Portugal; [5]Department of Dermatology, Unidade Local de Saúde de Coimbra (ULS), 3004-561 Coimbra, Portugal; [6]Department of Psychiatry, Unidade Local de Saúde de Coimbra (ULS), 3004-561 Coimbra, Portugal; [7]Coimbra Institute for Biomedical Imaging and Translational Research (CIBIT), University of Coimbra, 3000-548 Coimbra, Portugal; [8]Cytogenetics and Genomics Laboratory, Faculty of Medicine, University of Coimbra, 3000-548 Coimbra, Portugal; [9]Coimbra Institute for Clinical and Biomedical Research (iCBR), Center for Innovative Biomedicine and Biotechnology (CiBB), University of Coimbra, 3000-548 Coimbra, Portugal; [10]Faculty of Pharmacy, University of Coimbra, 3000-548 Coimbra, Portugal

Received January 28, 2025; Accepted April 2, 2025

DOI: 10.3892/ijmm.2025.5654

Abstract. Compromised cellular resilience in bipolar disorder (BD) has been associated with structural brain changes and cognitive deficits caused by perturbation of redox status, endoplasmic reticulum (ER) stress and innate immunity. These crucial cellular events are regulated by the ER-mitochondria close contacts at mitochondria-associated membranes (MAM) through Ca^{2+} transfer and lipids exchange between these organelles. The present study aimed to investigate the structural and functional alterations in MAM during BD early stages using patient- and control-derived cellular models, namely dermal fibroblasts. Morphological alterations in close ER-mitochondria contacts at MAM occur in BD cells and correlate with functional changes, as shown by lipid droplets accumulation. The MAM dysfunction in BD cells parallels changes in Ca^{2+} homeostasis, namely inhibition of store-operated Ca^{2+} entry (SOCE), ER Ca^{2+} depletion and attenuation of ER-mitochondria Ca^{2+} transfer, as well as enhanced ER and oxidative stress and NOD-like receptor family pyrin domain-containing 3 (NLRP3) inflammasome activation leading to sterile inflammation. The absence of inflammasome activation upon lipopolysaccharide exposure supports the compromised ability of BD cells (fibroblasts as well as monocytes) to deal with stressful conditions.

Correspondence to: Dr Cláudia Fragão Pereira, Center for Neuroscience and Cell Biology (CNC-UC), Center for Innovative Biomedicine and Biotechnology (CiBB), University of Coimbra, Rua Larga-Faculdade de Medicina, 1º andar, POLO I, 3004-504 Coimbra, Portugal
E-mail: cpereira@fmed.uc.pt

Abbreviations: AD, Alzheimer's disease; ASC, apoptosis-associated speck-like protein containing a C-terminal caspase-activation-and-recruitment (CARD) domain; ATF4, activating transcription factor 4; ATF6, activating transcription factor 6; BD, bipolar disorder; Ca^{2+}, calcium; CNS, central nervous system; ER, endoplasmic reticulum; GRP78, glucose-regulated protein 78; IMM, inner mitochondria membrane; iPSCs, induced pluripotent stem cells; IP3R, inositol trisphosphate receptor; LDs, Lipid droplets; LPS, lipopolysaccharide; MAM, mitochondria-associated membranes; MCU, mitochondrial Ca^{2+} uniporter protein; Mfn2, Mitofusin 2; SOD2, superoxide dismutase 2; NLRP3, NOD-like receptor family pyrin domain-containing 3; OMM, outer mitochondrial membrane; PLA, proximity ligation assay; PTPIP51, protein tyrosine phosphatase-interacting protein-51; RT-PCR, reverse transcriptase-polymerase chain reactions; ROS, reactive oxygen species; SCCI, single cell calcium imaging; SOCE, store-operated Ca^{2+} entry; SOD, superoxide dismutase; STIM1, stromal interaction molecule 1; TEM, transmission electron microscopy; TOM-20, Translocase of Outer Mitochondrial Membrane 20; ULS, Unidade Local de Saúde de Coimbra; UPR, unfolded protein response; VAPB, vesicle-associated membrane protein associated protein B; VDAC, voltage-dependent anion channel

Key words: mitochondria-associated membranes, endoplasmic reticulum, mitochondria, bipolar disorder, skin fibroblasts

In conclusion, MAM disruption is highlighted as a potential pathophysiological mechanism driving impaired cellular resilience in BD. Skin fibroblasts are a particularly attractive cellular model for studying mental illnesses, such as BD, due to the shared developmental origin of epidermal and neural tissues. The ectodermal origins of the skin-brain axis have been proposed as a novel route for understanding brain development, neurodevelopmental conditions and behavior modulation.

Introduction

Mitochondria and endoplasmic reticulum (ER) engage in intricate physical and biochemical interactions within specialized subcellular domains, the mitochondria-associated membranes (MAM), where their intermembrane distance is finely tuned to 10-20 nm (1,2). ER-mitochondria juxtaposition at MAM is mediated by tethering proteins including inositol trisphosphate receptor (IP3R), voltage-dependent anion channel (VDAC), Mitofusin 2 (Mfn2), vesicle-associated membrane protein-associated protein B (VAPB) and protein tyrosine phosphatase-interacting protein-51 (PTPIP51) (3,4). IP3R-VDAC and VAPB-PTPIP51 complexes, as well as Mfn2 and Sigma-1R, regulate ER-mitochondria Ca^{2+} flux (5-9). MAM are also enriched in lipid biosynthesis enzymes, namely those involved in lipid droplets (LDs) biogenesis (10,11). By regulating Ca^{2+} and lipid exchange, MAM govern pivotal cellular events, including mitochondrial bioenergetics and dynamics, redox balance, as well as ER stress and innate immune responses, namely NOD-like receptor family pyrin domain-containing 3 (NLRP3) inflammasome activation (4,12-14). Dynamic and responsive to cellular cues, MAM are vital platforms for intracellular homeostasis (15) and their dysfunction is implicated in various pathologies, including neurodegenerative diseases, metabolic and cardiovascular disorders and cancer, some of which are comorbidities of bipolar disorder (BD) (2,16-18).

BD is a chronic mental illness characterized by mood swings between mania and depression, affecting 1-2% of the world's population (19). Lifelong treatment is required (20), however, current drugs are limited and have notable side effects (21). BD diagnosis is complicated by the lack of specific biomarkers, emphasizing the need for a deeper understanding of its pathophysiology (20,22). Despite its neurobiology remaining unclear (20), anatomical and neuropathological examinations of the brains of patients with BD revealed abnormalities in the cellular resilience of neurons and glial cells towards stress (23). Disruptions in mitochondrial function and Ca^{2+} signaling, oxidative stress, apoptosis and perturbation of ER stress and immune responses are consistently reported in BD (23-27). Since these events are regulated by MAM (18,25), which play a pivotal role in coordinating cellular responses to stress, it was hypothesized that MAM impairment may underlie the diminished cellular resilience observed in BD. To test this, structural and functional changes resulting from ER-mitochondria miscommunication were assessed in dermal fibroblasts and monocytes from early-stage patients with BD compared with matched healthy controls.

Given the challenges of live brain tissue sampling, alternative *in vitro* models have emerged in BD research, using both non-neuronal cells (such as fibroblasts) and neuronal cells [such as olfactory neuronal epithelium and induced pluripotent stem cells (iPSCs) differentiated in a neuronal phenotype]. Several studies emphasize the occurrence of peripheral tissue alterations in various brain diseases (28-30). Moreover, patient-derived skin fibroblasts are a relevant BD cellular model due to: i) Sharing ontogenetic origin with the central nervous system (CNS) and expressing similar receptors and signaling pathways as neurons (31,32); ii) expressing genes implicated in psychiatric disorders (33); iii) easy accessibility through skin biopsies, with efficient establishment and maintenance in culture (32); iv) external factors (such as medication) disappearing after five passages (34); v) displaying molecular similarities with CNS cells, reflecting findings observed in brain tissue. Notably, the skin-brain axis is increasingly recognized as a dynamic interaction where changes in the skin not only mirror brain conditions but can also influence brain function. This bidirectional communication is rooted in the shared ectodermal origin of epidermal and neural tissues, with overlapping genetic, environmental and molecular risk factors shaping both systems (35). In the last decade, the skin-brain axis has been presented as a new perspective for understanding several diseases, including neurodevelopmental diseases such as autism spectrum disorder (35), neurodegenerative diseases such as Alzheimer's disease (AD) (36) and, more recently, behavioral changes such as depression and anxiety (37).

The present study, by investigating structural and functional alterations of MAM in dermal fibroblasts from patients with BD compared with matched healthy controls, identified increased ER-mitochondria juxtaposition at MAM in BD cells, which was associated with enhanced lipid transfer and formation of LDs, decreased ER-mitochondria Ca^{2+} exchange, as well as oxidative stress, ER stress-induced UPR and basal NLRP3 inflammasome activation. The present study revealed MAM as a potential pathophysiological mechanism driving impaired cellular resilience in BD and the skin-brain axis as a novel framework for studying the molecular mechanisms underlying BD pathophysiology.

Materials and methods

Culture of primary fibroblasts and monocytes. Dermal fibroblasts and peripheral blood (monocytes) were obtained from five male subjects diagnosed with early BD [stage 2 (38)] during euthymia and five age-(average age of 26±4.6) and gender-matched healthy controls, aged between 18-35 years old (Table SI). Participants were assessed regarding a DSM-5 BD criteria (39) through a validated diagnostic interview (40). This study was approved by the Ethics Committee of the Centro Hospitalar e Universitário de Coimbra (now ULS de Coimbra), reference 150/CES, July 3, 2018, and the samples were taken following written informed consent also approved by the same ethics committee (30). Dermal fibroblasts isolated from skin biopsies were maintained in HAM's F10 medium (cat. no. 31550-023; Thermo Fisher Scientific, Inc.) supplemented with 10% (v/v) heat-inactivated fetal bovine serum (FBS), 1% (v/v) antibiotic solution (10,000 U/ml penicillin, 10,000 μ/ml streptomycin) and 1% (v/v) L-Glutamine and AmnioMAX™-II Complete Medium (cat. no. 11269-016; Thermo Fisher Scientific, Inc.) in a proportion of 1:5. Cells were cultured in 75 cm^2 flasks and maintained in a humidified 5% CO_2-95% air atmosphere at 37˚C, with the medium

changed every 3 days. Cultures were passaged by trypsinization when cells reached 80-90% confluence. Fibroblasts with 6-16 passages were used for assays (41). Primary monocytes were isolated and cultured as previously described (42,43). Briefly, collected peripheral blood was carefully layered onto Ficoll-Paque Plus, followed by centrifugation to separate mononuclear cells. Monocytes ($CD14^+$ fraction) were then isolated using a magnetic separation system with the Human Monocyte Isolation kit II (Miltenyi Biotec), following the manufacturer's instructions. Primary monocytes were cultured in glutamine-free RPMI 1640 Medium (cat. no. 21870084 Gibco, Thermo Fisher Scientific, Inc.), supplemented with HEPES, 10% (v/v) heat-inactivated FBS, 100 U/ml penicillin, 100 μg/ml streptomycin, 2 mM glutamax, 1 mM sodium pyruvate, and 0.1 mM non-essentials amino acids. Cells were maintained at 37˚C in a humidified 5% CO_2 incubator.

Live cell imaging of ER-tracker and Mitotracker colocalization. Fibroblasts seeded for 48 h at a density of $0.1x10^5$ cells/cm^2 on 18 mm coverslips were loaded for 30 min at 37˚C with 0.1 μM Mitotracker Green (cat. no. m7514; Invitrogen; Thermo Fisher Scientific, Inc.) and 0.5 μM ER-tracker Red (cat. no. E34250 Thermo Fisher Scientific, Inc.) in Krebs medium (140 mM NaCl, 5 mM KCl, 1.2 mM Na_2HPO_4, 1 mM $MgCl_2$, 9.6 mM glucose, 20 mM Hepes, 1 mM $CaCl_2$, pH 7.4). Nuclei were stained with 15 μg/ml Hoechst 33342 for 5 min at room temperature (RT). Images were obtained using a Zeiss LSM 710 confocal microscope with plan-Apochromat 40x/1.4 objective (Zeiss AG). Colocalization of Mitotracker with ER-tracker was measured by using the Mander's coefficient of colocalization with the ImageJ v2.14 (National Institutes of Health) JACoP plugin (44). Mitochondrial area was calculated using the same plugin in Mitotracker Green images.

Confocal microscopy analysis of IP3R-VDAC colocalization. Fibroblasts were cultured for 48 h at a density of $0.1x10^5$ cells/cm^2, at 37˚C, in 12-well plates with 18 mm coverslips. Immunocytochemistry was performed as previously described (41). Briefly, cells were fixed with 4% (w/v) paraformaldehyde, pH 7.4, in PBS for 15 min. After permeabilization with 0.1% (v/v) Triton X-100 for 5 min, fibroblasts were blocked for 1 h with 3% (w/v) BSA prepared in 0.2% (v/v) Tween 20. Afterwards, cells were incubated overnight at 4˚C with mouse anti-VDAC1 (1:250; cat. no. ab14734; Abcam) and rabbit anti-IP3R (1:1,000; cat. no. ab5804; Abcam) primary antibodies. Cells were then incubated with the secondary antibodies Alexa Fluor 594 goat anti-rabbit (1:200; cat. no. A11012; Invitrogen; Thermo Fisher Scientific, Inc.) and Alexa Fluor 488 goat anti-mouse (1:200; cat. no. A11001; Invitrogen; Thermo Fisher Scientific, Inc.) for 1 h, at RT. Proximity ligation assay (PLA), using the Duolink reagents (cat. no. DUO92002/4-100RXN; MilliporeSigma), was used following the manufacturer's instructions. Cells were fixed with 4% (w/v) paraformaldehyde, pH 7.4, in PBS for 15 min. Permeabilization was performed using 0.1% (v/v) Triton X-100 in PBS for 5 min, and blocking was done with 3% (w/v) BSA prepared in 0.2% (v/v) Tween 20, for 1 h, at RT. After permeabilization, fibroblasts were incubated overnight at 4˚C with the mouse anti-VDAC1 (1:250; cat. no. ab14734; Abcam) and rabbit anti-IP3R (1:1,000; cat. no. ab5804; Abcam) primary antibodies, prepared in blocking solution. Cells were then incubated with plus and minus PLA probes (1:5) for 1 h at RT. The coverslips were incubated with ligase (1:40) for 30 min at RT, followed by incubation with polymerase (1:80) for 1 h and 20 min at RT. In both techniques, nuclei were stained with Hoechst 33342 (15 μg/ml) for 5 min at RT, and the coverslips were mounted using Aqua-Poly/Mount mounting medium (cat. no. 18606 Polysciences Inc.). Images were obtained using a Zeiss LSM 710 confocal microscope with plan-Apochromat 40x/1.4 objective (Zeiss AG). Colocalization of VDAC1 with the IP3R was measured with Mander's coefficient of colocalization through ImageJ v2.14 (National Institutes of Health) JACoP plugin (44). The particle analysis function of ImageJ was used to quantify the number of PLA red fluorescent spots per cell.

Transmission electron microscopy (TEM). Fibroblasts cultured for 48 h in a 100 mm cell culture dish were fixed with 2.5% (w/v) glutaraldehyde in 0.1 M sodium cacodylate buffer (pH 7.2) for 2 h, at RT. Post-fixation was performed using 1% (w/v) osmium tetroxide for 90 min. After rinsing in buffer and distilled water, 1% (w/v) aqueous uranyl acetate was added and incubated for 1 h, at RT, in the dark for contrast enhancement. Samples were embedded in 2% (w/v) molten agar, dehydrated in a graded ethanol series (30-100%) and then impregnated and embedded in Epoxy resin. Ultrathin sections (70 nm) were mounted on copper grids and stained with 0.2% (w/v) lead citrate for 7 min. Observations were carried out on a FEI-Tecnai G^2 Spirit BioTwin electron microscope (Thermo Fisher Scientific, Inc.) at 100 kV. ImageJ v2.14 (National Institutes of Health) was used to measure the ER-mitochondria distance in fibroblasts.

Western blot analysis of MAM components, Ca^{2+} channels and ER stress markers. Skin fibroblasts were lysed on ice with an ice-cold lysis RIPA buffer [250 mM NaCl, 50 mM Tris base, 1% (v/v) Nonidet P-40, 0.5% (v/v) sodium deoxycholate (DOC), 0.1% (v/v) Sodium Dodecyl Sulfate (SDS), pH 8.0] freshly supplemented with 2 mM DTT, 1% (v/v) protease inhibitor cocktail (cat. no. P2714; MilliporeSigma), and PhosSTOP™ (cat. no. 4906837001; MilliporeSigma). After 20 min on ice, nuclei and insoluble cell debris were removed by centrifugation at 18,000 x g for 10 min at 4˚C, and the supernatants were collected and stored at -20˚C until further use. The total protein amount of each sample was quantified using the Pierce bicinchoninic acid (BCA) assay kit (cat. no. 23225; Thermo Fisher Scientific, Inc.). Then, thirty micrograms of protein from total cell lysates were separated by electrophoresis in 10-12.5% SDS polyacrylamide gels (SDS/PAGE) and transferred to PVDF membranes (cat. no. ipvh00010; MilliporeSigma). After blocking with 5% (w/v) BSA during 1 h, at RT, membranes were incubated overnight, at 4˚C with the following primary antibodies: mouse anti-VDAC (1:1,000; cat. no. sc-390996; Santa Cruz Biotechnology, Inc.), rabbit anti-MCU (1:1,000; cat. no. 14997S; Cell Signaling Technology, Inc.), rabbit anti-STIM1 (1:1,000; cat. no. 11565-1-AP; Proteintech Group, Inc.), mouse anti-GRP78 (1:1,000; cat. no. 610978 BD Biosciences), rabbit anti-ATF4 (1:1,000; cat. no. 11815S; Cell Signaling Technology, Inc.), rabbit anti-ATF6 (1:1,000; cat. no. ab37149;

Abcam), mouse anti-Mfn2 (1:1,000; cat. no. sc-100560; Santa Cruz Biotechnology, Inc.), goat anti-Sigma-1R (1:1,000; cat. no. sc-22948; Santa Cruz Biotechnology, Inc.), rabbit anti-VAPB (1:1,000; cat. no. 14477-1-AP; Proteintech Group, Inc.), and rabbit anti-PTPIP51 (1:1,000; cat. no. 20641-1-AP; Proteintech Group, Inc.). Then membranes were incubated for 1 h, at RT, with HRP-conjugated goat anti-mouse IgG (1:20,000; cat. no. 31432; Thermo Fisher Scientific, Inc.), goat anti-rabbit IgG (1:20,000; cat. no. 31462; Thermo Fisher Scientific, Inc.) or rabbit anti-goat IgG (1:20,000; cat. no. 31402; Thermo Fisher Scientific, Inc.). The protein immunoreactive bands were visualized by chemiluminescence with the Pierce ECL Western Blotting Substrate (cat. no. 32106; Thermo Fisher Scientific, Inc.) in a Chemidoc Imaging System (Bio-Rad Laboratories, Inc.). The monoclonal anti-β-actin antibody (1:10,000; cat. no. A5441; MilliporeSigma) was used for protein loading control. The optical density of the bands was quantified with the Image Lab Software (Bio-Rad Laboratories, Inc.) (41). Stripping followed by reprobing with another antibody to label proteins of different molecular weight was performed in some membranes, as indicated in the figure legends.

Fluorescence microscopy quantification of lipid droplets and TOM-20. Fibroblasts cultured for 48 h at a density of $0.4x10^4$ cells/cm^2 in μ-slide 8 well plates (cat. no. 80806 Ibidi) were fixed with 4% (w/v) paraformaldehyde, pH 7.4 for 15 min, permeabilized with 0.1% (v/v) Triton X-100 for 5 min and blocked with 3% (w/v) BSA prepared in 0.05% (w/v) saponin for 1 h, at RT. Cells were then incubated overnight at 4˚C with the rabbit anti-translocase of outer mitochondrial membrane 20 (TOM20; 1:500; cat. no. sc-11415; Santa Cruz Biotechnology, Inc.) primary antibody and then with Alexa Fluor 488 goat anti-rabbit secondary antibody (1:200; cat. no. A11008; Invitrogen; Thermo Fisher Scientific, Inc.) for 1 h, at RT. After loading with the fluorescent probe LipidTOX red (1:200; cat. no. H34476; Invitrogen; Thermo Fisher Scientific, Inc.) for 2 h, nuclei were stained with Hoechst 33342 (15 μg/ml) for 5 min at RT and confocal images were obtained using a Zeiss LSM 710 confocal microscope (Zeiss AG) with a plan-Apochromat 40x/1.4 objective. The number of red spots (LDs)/cell was quantified using the Imaris Microscopy Image Analysis Software Spot function v10.2 (Oxford Instruments).

Single cell calcium imaging (SCCI). Fibroblasts seeded for 48 h on 18 mm coverslips at a density of $0.1x10^5$ cells/cm^2 were loaded for 30 min at 37˚C with 4 μM Fluo-4/AM (cat. no. F14201; Invitrogen; Thermo Fisher Scientific, Inc.) or 10 μM Rhod-2/AM (cat. no. R1244; Invitrogen; Thermo Fisher Scientific, Inc.), both prepared in solution A (135 mM NaCl, 5 mM KCl, 1 mM $MgCl_2$, 1 mM $MgSO_4$, 20 mM HEPES, 0.4 mM KH_2PO_4, 5.5 mM glucose and 1 mM $CaCl_2$, pH 7.4). After incubation, cells were kept in solution B (135 mM NaCl, 5 mM KCl, 1 mM $MgCl_2$, 1 mM $MgSO_4$, 20 mM HEPES, 0.4 mM KH_2PO_4, 5.5 mM glucose and 0.5 mM EGTA, pH 7.4), at 37˚C. Basal fluorescence was recorded every 20 sec for 2 min and upon stimuli with 100 μM histamine (cat. no. H7125; MilliporeSigma) the fluorescence was recorded every 1 sec for at least 4 min. In a Ca^{2+}-free medium, store-operated Ca^{2+} entry (SOCE) was analyzed upon induction of ER Ca^{2+} depletion with 1 μM thapsigargin (cat. no. T9033; MilliporeSigma) followed by the addition of 2 mM Ca^{2+} to promote the uptake of Ca^{2+} from the extracellular medium (45). Images were acquired using a Zeiss Cell Observer Spinning Disk microscope with plan-Apochromat 20x/0.8 objective (Zeiss AG).

Analysis of oxidative stress. Fibroblasts seeded for 48 h at a density of $0.4x10^4$ cells/cm^2 in μ-slide 8 well ibidi plates (cat. no. 80806 Ibidi) were loaded with 5 μM CellROX green (cat. no. C10444; Invitrogen; Thermo Fisher Scientific, Inc.) in Krebs medium for 30 min, at 37˚C. Live cell imaging was performed during 3 min using a Zeiss Cell Observer Z1 microscope with a plan-Apochromat 20x/0.8 objective (Zeiss AG). Fibroblasts cultured for 48 h at a density of $0.1x10^5$ cells/cm^2 were incubated with 10 μM MitoPY (cat. no. SML0734; MilliporeSigma) in Krebs medium for 30 min at 37˚C. Basal fluorescence values were measured for 5 min in a fluorimeter SpectraMax Gemini EM microplate reader set to 503 nm excitation and 540 nm emission wavelengths. Values were normalized to the protein amount. An enzymatic superoxide dismutase (SOD) assay kit (cat. no. 19160-1KT-F; MilliporeSigma) was used to determine the activity of the mitochondrial isoform of SOD, the superoxide dismutase 2 (SOD2) in primary fibroblasts derived from patients with BD and healthy subjects, according to the manufacturer's instructions. For this purpose and as previously described (42), fibroblasts were lysed on RIPA buffer [250 mM NaCl, 50 mM Tris base, 1% (v/v) Nonidet P-40, 0.5% (v/v) sodium deoxycholate (DOC), 0.1% (v/v) Sodium Dodecyl Sulfate (SDS), pH 8.0], without supplements. The total activity of SOD and particular the activity of SOD2 were differentiated by the inclusion of 2 mM potassium cyanide (KCN), which selectively inhibits cytosolic isoform of SOD antioxidant enzyme, the superoxide dismutase 1 (SOD1). The plate was then incubated at 37˚C for 20 min, and the absorbance was read in a spectrophotometer Spectramax plus 384 microplate reader (BioTek Instruments) set to 450 nm. Values were normalized to the protein amount determined by the BCA method.

Reverse transcription-quantitative (RT-q) PCR quantification of pro-inflammatory mediators. Fibroblasts were plated at a density of $0.5x10^5$ cells/cm^2 and stabilized for 24 h. RNA was extracted with the NZYol reagent (cat. no. MB18501; Nzytech), and its concentration was measured using a NanoDrop 2000c Spectrophotometer (Thermo Fisher Scientific, Inc.). Samples were stored at -80˚C for subsequent use. Briefly, the total RNA (2 μg per sample) was reverse transcribed into cDNA using the NZY First-Strand cDNA Synthesis kit (cat. no. MB12502; Nzytech). Then, RT-qPCR were performed, in triplicate for each sample, using the NZYSpeedy qPCR Green Master Mix Kit (cat. no. MB22403; Nzytech), in the CFX Connect RT-PCR Detection System (Bio-Rad Laboratories, Inc.), as previously described (46). Briefly, samples were denatured at 95˚C for 3 min. 40 cycles were run for 10 sec at 95˚C for denaturation, 30 sec at 55˚C for annealing and 30 sec at 72˚C for elongation. After amplification, a threshold was set for each gene, and Cq values were calculated for all the samples (47). Gene expression changes were analyzed using the CFX Maestro 1.1 system software (Bio-Rad Laboratories, Inc.). The primer sequences

were designed using the Beacon Designer software version 7.7 (Premier Biosoft International), and were thoroughly tested. The forward (F) and reverse (R) primers used were indicated in Table SII (Eurofins Scientific). Hprt-1 was used as a housekeeping gene to normalize the results of the genes of interest.

Colorimetric determination of caspase-1 activity. After 24 h of stabilization, the culture medium of plated fibroblasts at a density of $0.5x10^5$ cells/cm^2 was replaced by FBS-free HAM's F10 medium and cells were exposed to 5 μg/ml lipopolysaccharide (LPS) for 32 h or were kept in FBS-free HAM's F10 medium. Fibroblasts were then lysed in lyses buffer (25 mM HEPES, 1 mM EDTA, 1 mM EGTA, 2 mM $MgCl_2$, pH 7.5) through consecutive series of freezing/thawing in liquid N_2. Proteins (100 μg/ml) were incubated with 4 mM caspase-1 substrate (cat. no. SCP0066; MilliporeSigma) in buffer [25 mM HEPES, 10% (w/v) sucrose, pH 7.5] freshly supplemented with 0.1% (w/v) CHAPS and 10 mM DTT. After 2 h of incubation at 37˚C, absorbance was measured at 405 nm in a standard Synergy HT Multi Detection Microplate Reader.

ELISA measurement of secreted IL-1β levels. Fibroblasts and monocytes were seeded at a density of $0.5x10^5$ cells/cm^2 and $0.12x10^6$ cells/well, respectively. Culture medium was then replaced by FBS-free medium and cells were exposed to LPS at a concentration of 5 μg/ml (fibroblasts) or 1 μg/ml (monocytes) for 32 h or kept in FBS-free medium. After concentrating fibroblast supernatants with concentration columns (cat. no. VS0192; Sartorius AG), IL-1β secretion was quantified by ELISA kit (cat. no. 437004; BioLegend, Inc.) following manufacturer's instructions (42,43). Absorbance values were measured in a standard Synergy HT Multi Detection Microplate Reader (BioTek Instruments) set to 450 nm wavelength. IL-1β levels were expressed as pg/ml in the case of fibroblasts and as values normalized to the baseline values in the case of monocytes. For both cells, the results were also presented as fold increase calculated by the difference between the LPS-treated and baseline values.

Data analysis. Results were expressed as mean ± standard error of the mean. Normality was assessed by the D'Agostino and Pearson and Shapiro-Wilk tests. Statistical analysis was performed by using the parametric unpaired Student's t-test or the Mann-Whitney non-parametric test. A two-way ANOVA test followed by Tukey's or Sidak's post-hoc test was used for multiple comparisons with two factors. Statistical analysis was performed using the GraphPad Prism software 9.0 (Dotmatics). $P<0.05$ was considered to indicate a statistically significant difference.

Results

Tight ER-mitochondria juxtaposition in BD fibroblasts. To investigate alterations in ER-mitochondria apposition in fibroblasts derived from patients with BD and healthy controls, the colocalization between the ER (ER-Tracker) and mitochondria (Mitotracker) was assessed by confocal microscopy (Fig. 1A). BD fibroblasts exhibited increased ER-mitochondria colocalization compared with controls (Fig. 1B). This observation was corroborated by results demonstrating higher proximity between IP3R (ER marker) and VDAC (mitochondria marker; Fig. 1C and D), as well as by a rise in the number of PLA dots, which results from enhanced IP3R-VDAC contacts points, in BD fibroblasts compared with controls (Fig. 1E and F), strongly suggesting increased ER-mitochondria contacts in this BD cellular model. Furthermore, the contact sites between the ER and mitochondria (≤80 nm) were quantified by TEM (Fig. 1J). A significant reduction in the physical distance between both organelles was identified in BD fibroblasts compared with controls (Fig. 1K). The distribution of those contacts clear demonstrate that BD fibroblasts exhibit a markedly higher percentage of close contacts ≤20 nm (MAM) and a lower percentage of long contacts >20 nm, in comparison with control cells (Fig. 1L). Together, the findings obtained using different microscopy approaches suggested increased ER-mitochondria close contacts sites (MAM) in fibroblasts derived from patients with BD. Notably, these alterations are independent of changes in the number and area of mitochondria (Fig. 1G-I). To investigate whether MAM upregulation in fibroblasts derived from patients with BD is associated with changes in ER-mitochondria tethers, the protein levels of key MAM tethering complexes, specifically Mfn2 (Fig. 2A and B), VDAC (Fig. 2C and D), VAPB (Fig. 2G and H) and PTPIP51 (Fig. 2K and L), were assessed by western blotting. A significant rise in VDAC levels (Fig. 2C and D) and a qualitative, though not statistically significant, increase in PTPIP51 content (Fig. 2K and L) was observed in BD fibroblasts compared with control cells.

Altered lipid metabolism and calcium homeostasis in BD fibroblasts. Given the pivotal role of MAM in the transfer of Ca^{2+} and lipids between the ER and mitochondria, the present study then evaluated MAM function in control and BD fibroblasts, by examining lipid metabolism and Ca^{2+} fluxes (4,12-14).

The content of LDs was assessed as an indicator of the efficacy of ER-mitochondria lipid transfer and, therefore, as a measure of MAM function (10). The quantity of LDs was evaluated by using lipidTOX, a fluorescent probe with high affinity for LDs (Fig. 3A). Quantitative analysis demonstrated a notable enhancement in the number of LDs per cell in BD fibroblasts compared with control cells (Fig. 3B), suggesting a correlation between upregulated MAM and enhanced lipid metabolism in BD.

The IP3R-mediated ER-mitochondria Ca^{2+} transfer was determined by using Rhod-2AM, a mitochondrial Ca^{2+} indicator. Notably, BD fibroblasts stimulated with the IP3R agonist histamine exhibited a significant reduction in mitochondrial Ca^{2+} uptake compared with controls (Fig. 3D and F), despite the decreased ER-mitochondria distance in BD cells. The data showed that these differences were not due to downregulation of the mitochondrial calcium uniport (MCU) at IMM, which aligns with the ER IP3R and VDAC at outer mitochondrial membrane (OMM) to facilitate the transfer of Ca^{2+} into mitochondria (48), since similar protein levels were detected in both control and BD cells (Fig. 3J and K). Furthermore, they were not associated with alterations in Sigma-1R, a modulator of IP3R-mediated ER-mitochondria Ca^{2+} transfer, since its protein levels were not affected in BD (Fig. 2K and M). The alterations in the ER-mitochondria Ca^{2+} transfer observed between control and BD cells might instead arise from compromised

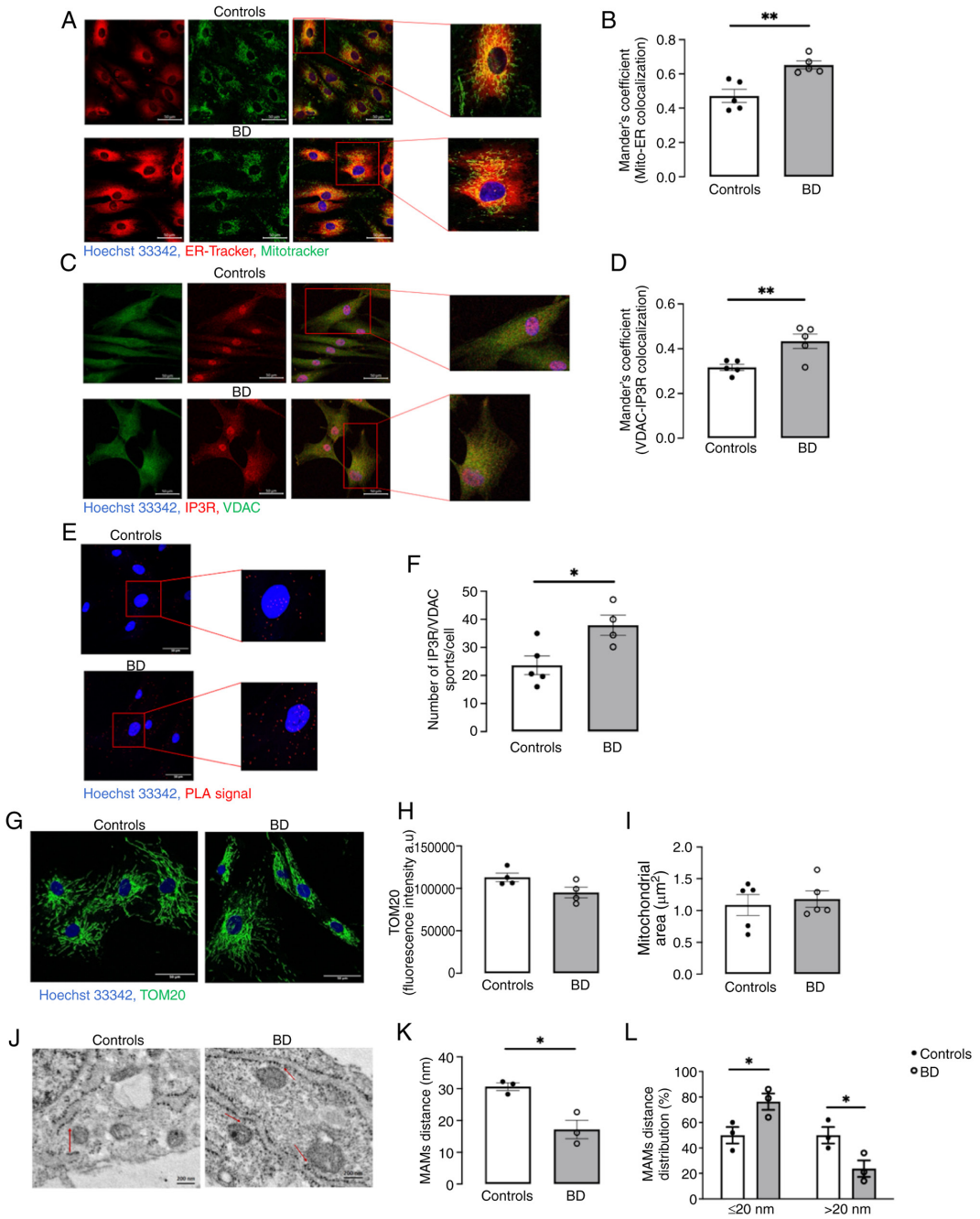

Figure 1. ER-mitochondria contacts in primary fibroblasts derived from patients with BD and healthy controls. Colocalization of Mitotracker and ER-Tracker fluorescent probes was evaluated by live cell imaging. (A) Representative confocal microscopy images of Mitotracker (green) and ER-Tracker (red) immunoreactivity and nuclei labelling with Hoechst 33342 (blue; scale bar, 50 μm). (B) The mitochondrial fraction (Mitotracker) that colocalizes with the ER (ER-Tracker) was measured with the Mander's coefficient of colocalization using the ImageJ software. Colocalization of the IP3R (ER marker) and the VDAC (mitochondrial marker) was evaluated by immunocytochemistry. (C) Representative confocal microscopy images of VDAC (green) and IP3R (red) immunoreactivity and nuclei labelling with Hoechst 33342 (blue; scale bar, 50 μm). (D) The mitochondrial fraction (VDAC) that colocalizes with the ER (IP3R) was measured with the Mander's coefficient of colocalization (ImageJ software). Data represent the means ± standard error of the mean of results obtained by the analysis of five images from five participants per group. The number of IP3R/VDAC dots per cell was determined by the PLA. (E) Representative confocal microscopy images of PLA signal IP3R/VDAC dots (red) and nuclei labelling with Hoechst 33342 (blue; scale bar, 50 μm). (F) PLA fluorescent quantification was performed using the Particle Analysis function of ImageJ software. Data represent the means ± standard error of the mean of results obtained by the analysis of five images from five controls and four patients. The mitochondrial network was analyzed by immunocytochemistry. (G) Representative confocal microscopy images of TOM20 immunoreactivity (green) and Hoechst 33342-stained nuclei (blue; scale bar, 50 μm). (H) TOM20 staining was analyzed using the ImageJ software. Data represent the means ± standard error of the mean of results obtained by the analysis of five images collected from four participants per group. (I) The mitochondrial area was quantified in the confocal images of Mitotracker (Fig. 1A) using a macro designed in the ImageJ software. Statistical significance of differences between experimental groups was determined by unpaired Student's t-test. The ER-mitochondria contacts were evaluated by transmission electron microscopy. (J) Representative images of the ER-mitochondria contacts (arrow; scale bar, 200 nm). (K) ER-mitochondria distance was measured using the ImageJ software. (L) Distribution of the ER-mitochondria contacts: close contacts (≤20 nm; MAM) and large contacts (>20 nm). Data represent the means ± standard error of the mean of results obtained by the analysis of at least five images collected from three participants per group. Statistical significance between groups was determined using the unpaired Student's t-test *P<0.05, **P<0.01; and the comparison of close (≤20 nm) and large contacts (>20 nm) between the two groups was obtained using the two-way ANOVA test, followed by the Sidak's post hoc test: *P<0.05. ER, endoplasmic reticulum; BD, bipolar disorder; IP3R, inositol trisphosphate receptor; VDAC, voltage-dependent anion channel; PLA, proximity ligation assay; TOM20, translocase of outer mitochondrial membrane 20; MAM, mitochondria-associated membranes.

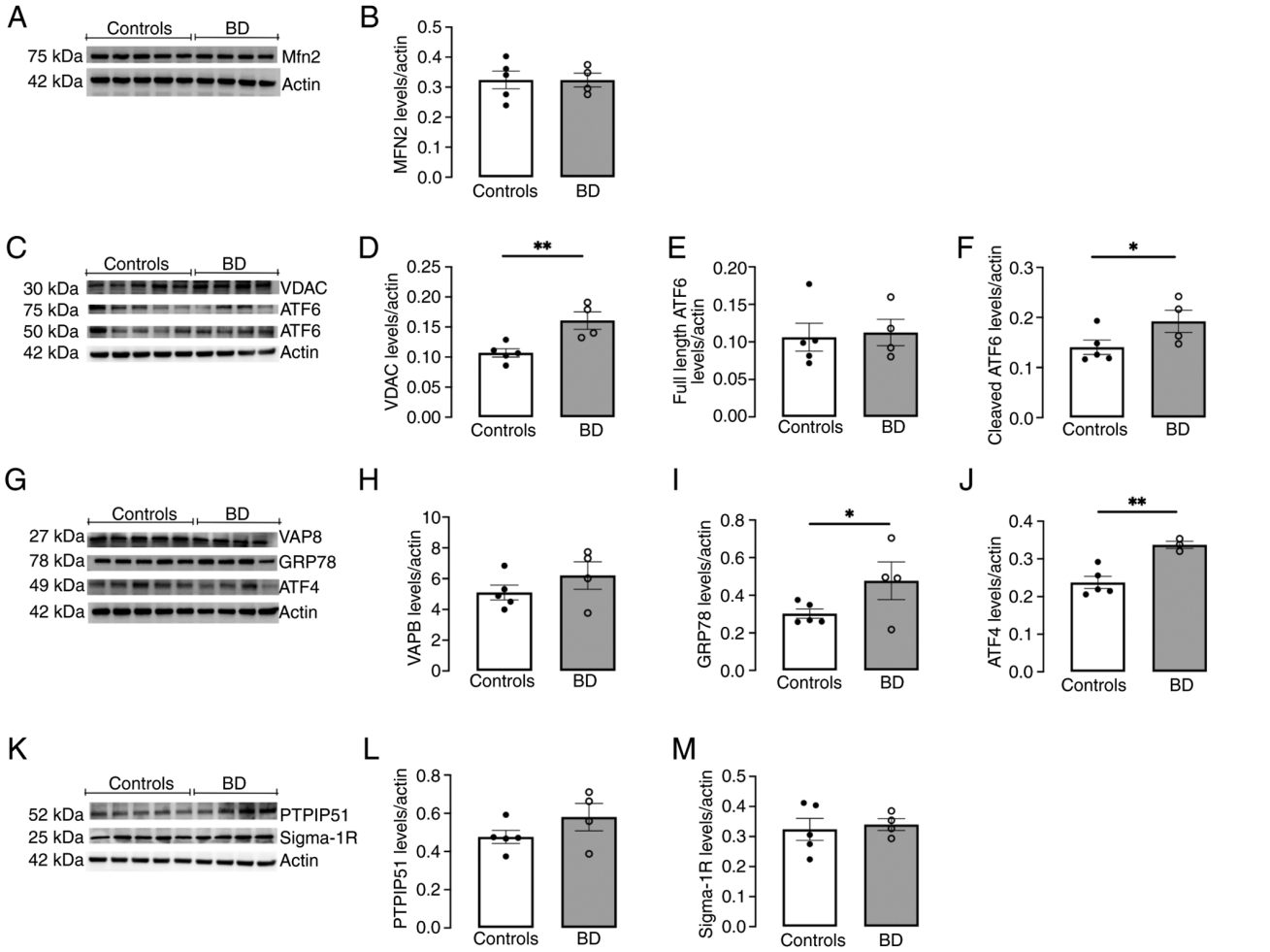

Figure 2. Levels of components of ER-mitochondria contacts (Mfn2, VDAC, VAPB, PTPIP51 and Sigma-1R) and ER stress-induced UPR markers (GRP78, ATF4 and ATF6) in primary fibroblasts derived from patients with BD and healthy controls. Protein levels of (A and B) Mfn2, (C and D) VDAC, (C, E and F) ATF6, (G and H) VAPB, (G and I) GRP78, (G and J) ATF4, (K and L) PTPIP51 and (K and M) Sigma-1R, were quantified by western blotting in total cellular extracts obtained from primary fibroblasts derived from patients with BD and healthy controls. β-actin was used to control protein loading and to normalize the levels of the proteins of interest. Data represent the means ± standard error of the mean of results obtained in samples from five healthy controls and four patients with BD. Statistical differences between fibroblasts from patients with BD and healthy controls were analyzed using the unpaired Student's t-test: *P<0.05, **P<0.01. (A) The Mfn2 antibody was incubated in the first western blotting. VDAC and ATF6 antibodies were both incubated in the second western blotting. (C) The ATF6 antibody, which recognizes both full-length (75 kDa) and cleaved protein (50 kDa), was incubated on the VDAC western blotting membrane, after a stripping procedure. (G) The VAPB, GRP78 and ATF4 antibodies were labelled on the third western blotting. Upon incubation with the VAPB antibody, the western blotting membrane was then incubated with ATF4 and GRP78, after a stripping. (K) PTPIP51 and Sigma-1R antibodies were both incubated in the fourth western blotting. The Sigma-1R antibody was incubated on the PTPIP51 western blotting membrane, after a stripping. ER, endoplasmic reticulum; UPR, unfolded protein response; BD, bipolar disorder; MAM, mitochondria-associated membranes; Mfn2, Mitofusin 2; VDAC, voltage-dependent anion channel; VAPB, vesicle-associated membrane protein associated protein B; PTPIP51, protein tyrosine phosphatase-interacting protein-51; GRP78, glucose-regulated protein 78; ATF4. activating transcription factor 4; ATF6-activating transcription factor 6.

IP3R-mediated ER Ca^{2+} release, since the cytosolic Ca^{2+} levels measured with Fluo-4/AM in histamine-stimulated BD fibroblasts were lower compared with those of control cells (Fig. 3C and E). This diminished release observed in BD cells can result from a deficient replenishment of Ca^{2+} in the ER lumen by SOCE-mediated extracellular Ca^{2+} influx, which in turn can modulate mitochondrial Ca^{2+} uptake (49,50). To evaluate SOCE, fibroblasts were loaded with Fluo-4/AM in Ca^{2+}-free medium and stimulated with thapsigargin, an inhibitor of the Sarco/endoplasmic reticulum Ca^{2+}-ATPase (SERCA) pump, to assess ER Ca^{2+} release, followed by the addition of extracellular Ca^{2+} to investigate SOCE-mediated Ca^{2+} entry. The analysis of ER Ca^{2+} content in thapsigargin-stimulated cells revealed the depletion of ER Ca^{2+} and impaired SOCE-dependent Ca^{2+} influx in BD fibroblasts compared with controls (Fig. 3G-I). These observations suggested that the reduced ER-mitochondria Ca^{2+} transfer in BD cells resulted from the depletion of ER Ca^{2+} stores caused by impaired Ca^{2+} influx from the extracellular space through the SOCE pathway, which fails to replenish the ER. Notably, the BD-associated SOCE impairment is not due to alterations in the protein levels of stromal interaction molecule 1 (STIM1), a key component of the SOCE machinery (Fig. 3J and L).

Overall, the results showed that the proximity between the ER and mitochondria at MAM in BD cells was intimately linked to increased lipid exchange and biogenesis of LDs, but not with stimulation of the ER-mitochondria Ca^{2+} transfer.

Impaired redox status in BD fibroblasts. MAM play a crucial role in cellular redox status, maintaining a dynamic equilibrium

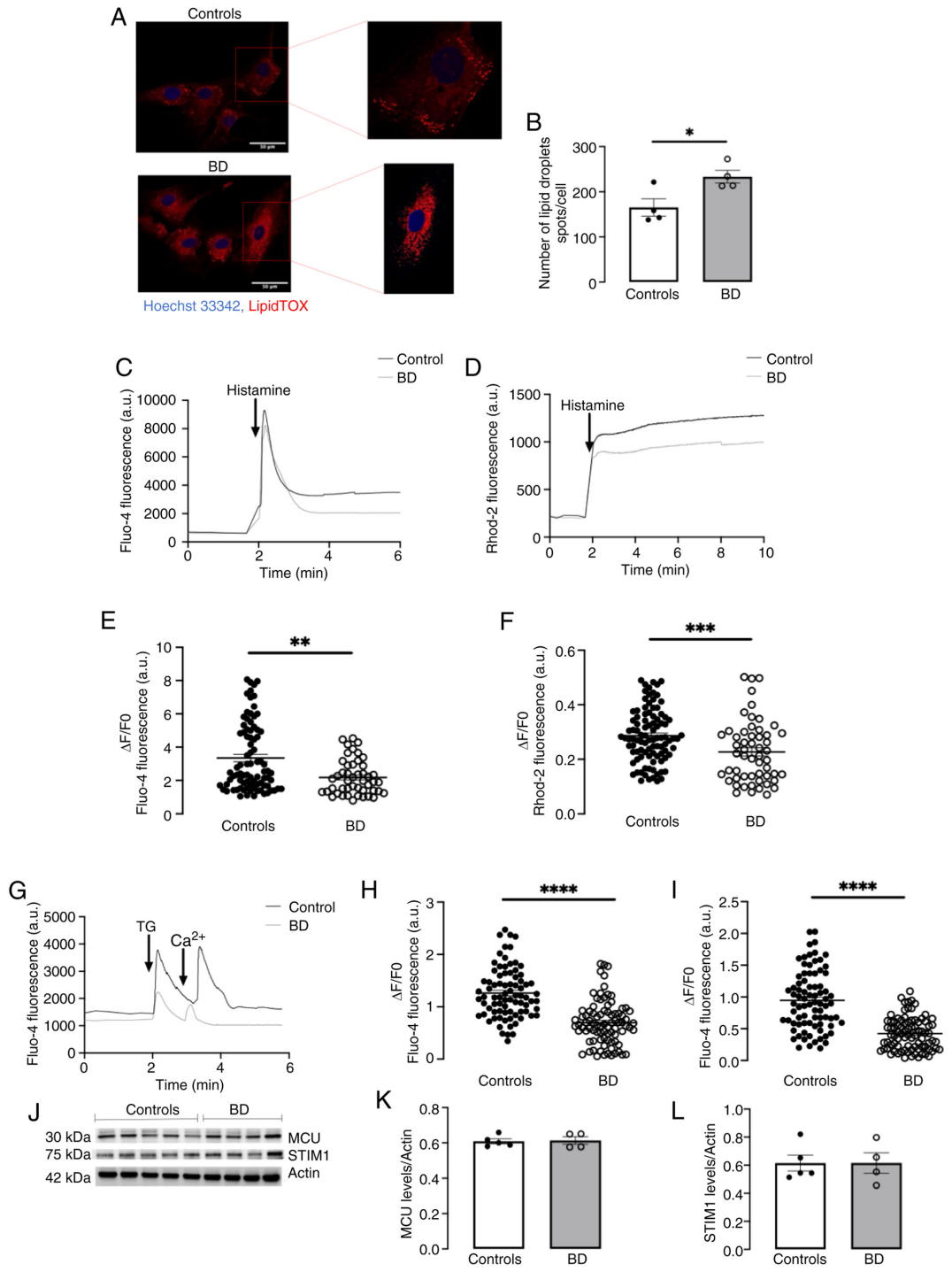

Figure 3. Lipid droplets accumulation and Ca^{2+} dynamics in primary fibroblasts derived from patients with BD and healthy controls. The number of lipid droplets per cell was determined using the LipidTOX fluorescent probe. (A) Representative confocal microscopy images of lipid droplets spots (red) and nuclei labelling with Hoechst 33342 (blue; scale bar, 50 μm). (B) Quantification of LipidTOX fluorescent was performed using the Spot function of Imaris Microscopy Image Analysis Software. Data represent the means ± standard error of the mean of results obtained by the analysis of at least five images collected from four participants per group. IP3R-mediated ER Ca^{2+} efflux and its influx into mitochondria were measured by SCCI with the fluorescent probes (C) Fluo-4 and (D) Rhod-2, respectively, after treatment with histamine (100 μM). (E and F) The SCCI results were baseline-corrected and normalized to calculate the normalized fluorescent calcium signals. Data were expressed as ΔF/F0, where ΔF=F-F0. F represents the highest post-stimulus value and F0 the mean baseline level. Data represent the means ± standard error of the mean of results obtained from 15-30 cells from each of the four participants per group. (G) SOCE was evaluated by measuring Ca^{2+} oscillations with Fluo-4 after thapsigargin (1 μM, TG)-induced ER Ca^{2+} depletion in Ca^{2+}-free medium and after addition of 2 mM $CaCl_2$ to the extracellular medium. (H and I) The SCCI results were baseline-corrected and normalized to calculate the normalized fluorescent calcium signals. Data were expressed as ΔF/F0, where ΔF=F-F0. F represents the highest post-stimulus value and F0 the mean baseline level. Data represent the means ± standard error of the mean of results obtained from 15-30 cells from each of the four participants per group. (J and K) MCU and (J and L) STIM1 protein levels were evaluated in total cellular extracts obtained from control and BD fibroblasts through western blotting. β-actin was used to control protein loading and to normalize the levels of the proteins of interest. Data represent the means ± standard error of the mean of results obtained in samples from five healthy controls and four patients with BD. The STIM1 antibody was incubated on the Sigma-1R western blotting membrane, after a stripping. Statistical difference between groups was evaluated with unpaired Student's t-test (B, D, H, I and L) or with Mann-Whitney non-parametric test (F and K): *P<0.05; **P<0.01; ***P<0.001; ****P<0.0001. BD, bipolar disorder; IP3R, inositol trisphosphate receptor; ER, endoplasmic reticulum; SCCI, single cell calcium imaging; STIM1, stromal interaction molecule 1; MCU, mitochondrial Ca^{2+} uniporter protein.

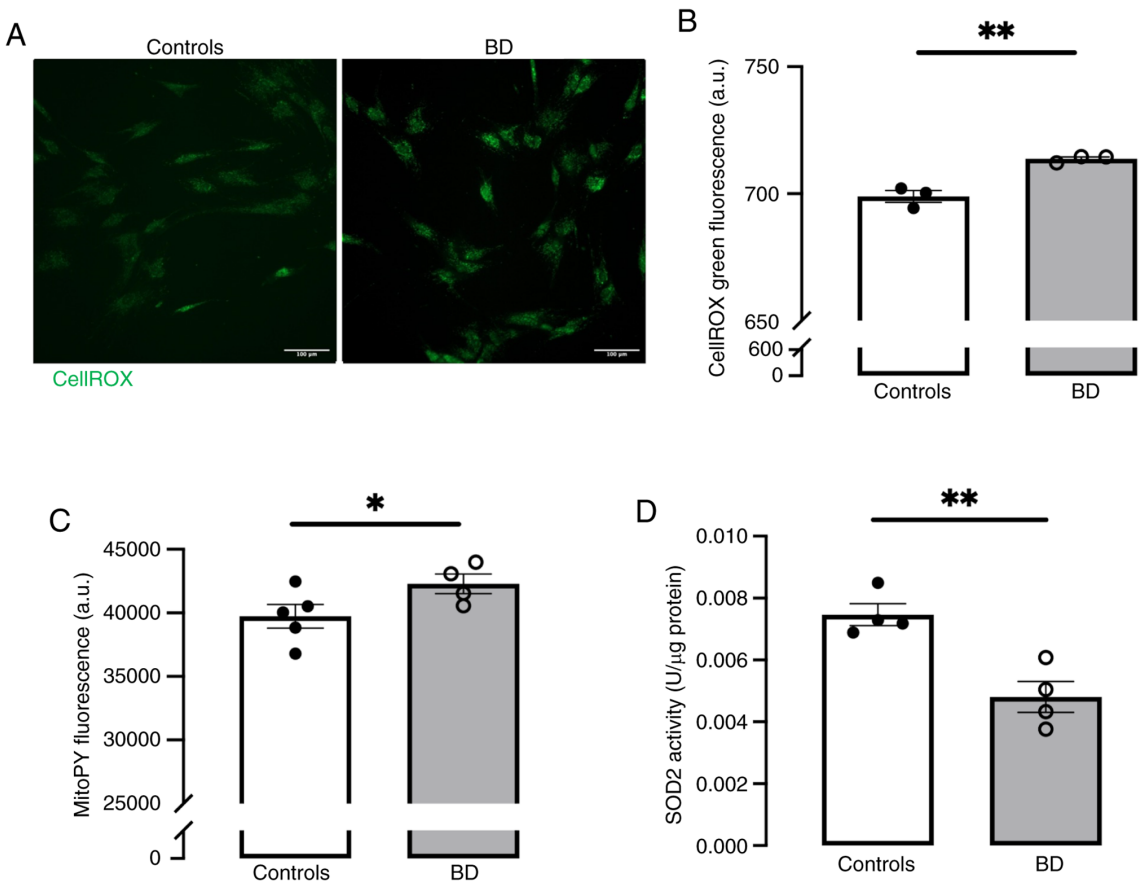

Figure 4. Redox state in primary fibroblasts derived from patients with BD and healthy controls. The accumulation of ROS in control and BD fibroblasts was assessed using the CellROX fluorescent probe. (A) Representative microscopy images of CellROX immunoreactivity (green; scale bar, 100 μm). (B) Quantification of the CellROX green staining using ImageJ software. Data represent the means ± standard error of the mean of results obtained in cells from three participants per group. At least five images from each participant were analyzed. (C) The levels of mitochondrial ROS were measured by using the MitoPY fluorescent probe. Data represent the means ± standard error of the mean of results obtained in cells from five healthy controls and four patients with BD. (D) The activity of SOD2 mitochondrial antioxidant enzyme was analyzed in primary fibroblasts derived from patients with BD and healthy controls by using a commercial kit. Data represent the means ± standard error of the mean of results obtained in total lysates obtained from cells isolated from four participants per group. The statistical significance of differences between control and BD fibroblasts was determined using the unpaired Student's t-test: *P<0.05; **P<0.01. BD, bipolar disorder; ROS, reactive oxygen species; SOD2, superoxide dismutase 2.

between reactive oxygen species (ROS) production and antioxidant defenses (51). To assess oxidative stress in fibroblasts derived from controls and patients with BD, ROS levels were measured using CellROX and the mitochondrial-specific MitoPY probes. A significant increase in ROS levels was observed (Fig. 4A and B) that are, at least in part, generated in mitochondria (Fig. 4C), probably due to the inhibition of SOD2 mitochondrial antioxidant enzyme (Fig. 4D).

ER stress-induced unfolded protein response (UPR) markers in BD fibroblasts. The ER-mitochondria communication at MAM coordinates cellular stress responses, particularly the UPR (52). A notable upregulation in the protein levels of several UPR markers, namely GPR78 (Fig. 2G and I), activating transcription factor 4 (ATF4) (Fig. 2G and J) and fragmented activating transcription factor 6 (ATF6) (Fig. 2C and F), was found in BD cells compared with controls, indicating ER stress induction in these patients.

Sterile inflammation in fibroblasts and monocytes derived from patients with BD. MAM provide a physical platform for NLRP3 inflammasome assembly by facilitating the communication among its components: NLRP3, caspase-1 and ASC (53,54). Activation of the NLRP3 inflammasome induces a signaling cascade culminating in the release of pro-inflammatory mediators such as interleukin-1 beta (IL-1β) (14,55). This cytosolic complex is activated by MAM-derived signals, namely danger signals released by dysfunctional mitochondria including ROS (13,14). Given the upregulation of MAM and significant ROS accumulation in BD fibroblasts, it is hypothesized that NLRP3 is activated in these cells playing a role in maintaining a potent chronic inflammatory environment (56).

Increased mRNA levels of NLRP3 and pro-IL-1β assessed by RT-qPCR (Fig. 5A and B), coupled with enhanced caspase-1 activity (Fig. 5F), in fibroblasts from patients with BD compared with controls, suggested NLRP3 inflammasome activation and sterile inflammation in BD. The upregulation of other pro-inflammatory cytokines, including TNFα, IL-6 and IL-8 detected in BD fibroblasts (Fig. 5C-E), provided strong evidence for a BD-associated inflammatory state. Then, NLRP3 inflammasome activation was evaluated under LPS-induced inflammation-prone conditions, by quantifying secreted IL-1β levels, the classical readout of NLRP3 activation. A notable rise in IL-1β secretion was observed in

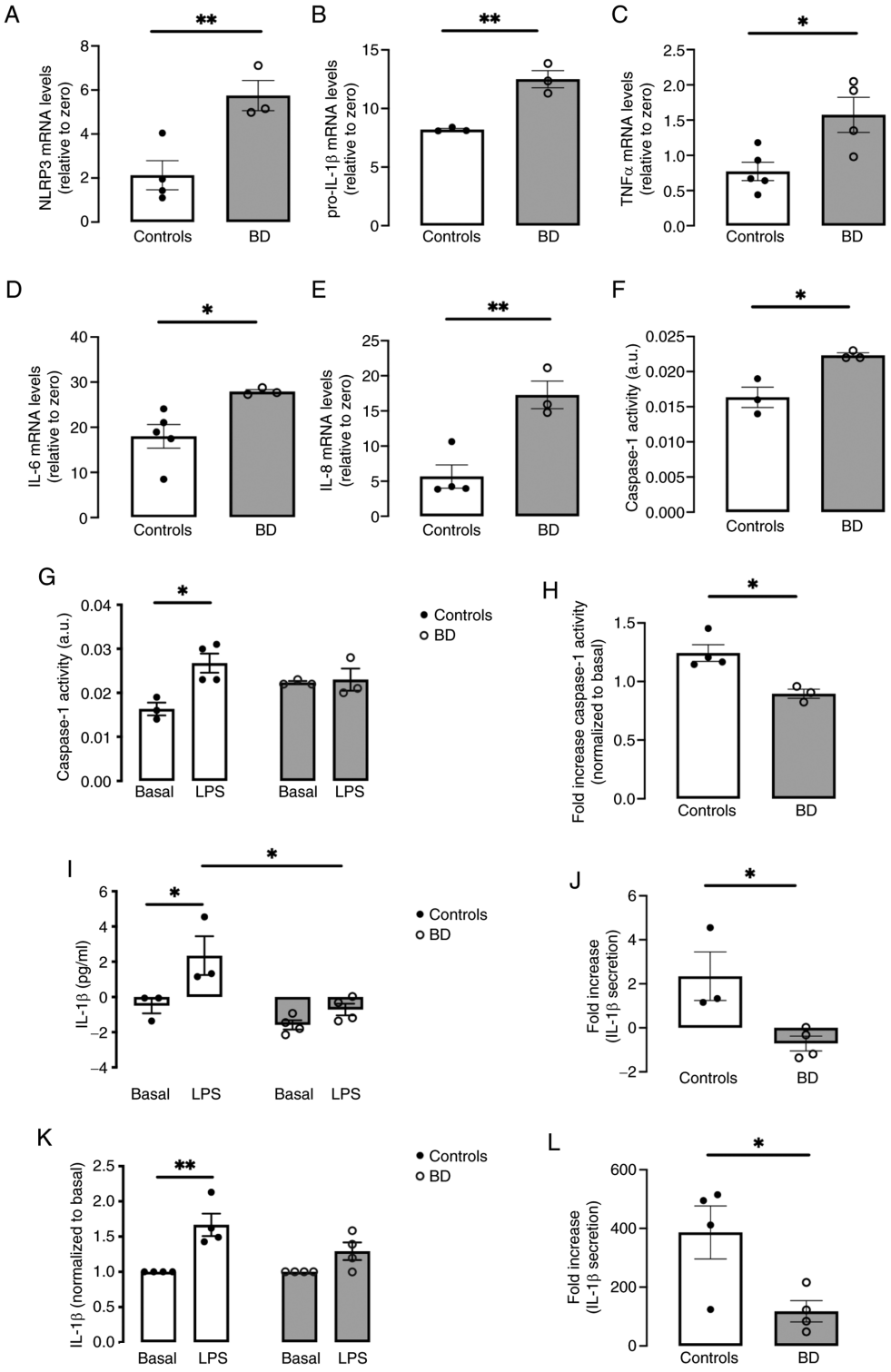

Figure 5. NLRP3 inflammasome activity and inflammatory status in primary fibroblasts and monocytes derived from patients with BD and healthy controls. Basal mRNA levels of (A) NLRP3 and pro-inflammatory cytokines (B) pro-IL-1β, (C) TNFα, (D) IL-6 and (E) IL-8 were evaluated by reverse transcription-quantitative PCR in fibroblasts from patients with BD and healthy controls. (F) Baseline levels of caspase-1 activity in control and BD fibroblasts. (G) Caspase-1 activity was analyzed in total extracts from control and BD fibroblasts treated in the absence or presence of 5 μg/ml LPS for 32 h. (H) Fold increase of caspase-1 activity was calculated by normalizing the levels of caspase-1 activity in control and BD fibroblasts treated with LPS to the baseline values. Data represent the means ± standard error of the mean of results obtained in cells from 3-5 participants per group. (I) IL-1β levels in supernatants from control and BD fibroblasts incubated in the presence or absence of 5 μg/ml LPS for 32 h, were quantified using an ELISA kit an expressed as pg/ml. (J) Fold increase of IL-1β secretion was calculated by the difference between LPS-treated and basal values. Data represent the means ± standard error of the mean of results obtained in cells from three controls and four patients with BD. (K) IL-1β levels in supernatants from primary monocytes derived from healthy controls and patients with BD incubated in the presence or absence of 1 μg/ml LPS for 32 h, were quantified by ELISA. Results were normalized to the basal levels and represent the means ± standard error of the mean of results obtained in cells from four participants per group. (L) IL-1β secretion in monocytes was also calculated as the fold increase observed upon LPS treatment. Data represent means ± standard error of the mean of results obtained in cells from four participants per group. Statistical significance of differences between groups was determined by the unpaired Student's t-test (A-F, H, J and L): *P>0.05; **P>0.01; significance between both basal and LPS-treated cells within each experimental group and between the two groups were obtained using the two-way ANOVA test, followed by the Tukey's post hoc test (G, I and K): *P>0.05; **P>0.01. NLRP3, NOD-like receptor family pyrin domain-containing 3; BD, bipolar disorder; LPS, lipopolysaccharide.

control fibroblasts treated with LPS for 32 h compared with untreated control cells, which was not observed in BD cells (Fig. 5I). This distinct pattern of response to LPS was reinforced upon examining the stimulated release of IL-1β, with a statistically significant decrease observed in BD fibroblasts (Fig. 5J). Comparable outcomes were found in fibroblasts from patients with BD and healthy subjects exposed to LPS for 12 h (data not shown). Moreover, a marked increase in caspase-1 activity was identified in LPS-exposed control fibroblasts, a response not observed in treated BD fibroblasts (Fig. 5G). Comparing the fold increase of caspase-1 in LPS-treated controls and BD fibroblasts reveals a substantial reduction in the later (Fig. 5H). Lastly, IL-1β secretion was quantified in primary monocytes isolated from the peripheral blood of both patients with BD and healthy controls, exposed to LPS for 32 h. Similarly, these innate immune cells also exhibited a deficient NLRP3 inflammasome activation when exposed to LPS (Fig. 5K and L).

Together, these findings illustrated that, under basal conditions, patients with BD manifest a pro-inflammatory state characterized by the upregulation of pro-inflammatory cytokines. However, the response of the NLRP3 inflammasome to an inflammatory stimulus is compromised in BD-derived cells, indicating that these individuals are less responsive to inflammation-prone conditions.

Discussion

The disruption of ER-mitochondria crosstalk at MAM has been linked to the onset and progression of various human pathologies, including cancer, neurodegenerative disorders, and metabolic and cardiovascular diseases (2,16-18), some of which are comorbidities of BD. MAM play a crucial role in essential biological functions, namely lipid metabolism, calcium homeostasis, mitochondrial bioenergetics and dynamics, redox balance and control over ER stress and inflammatory responses (15,52). These MAM-related cellular events are disrupted in BD (25), suggesting a link between MAM alterations and BD pathophysiology. Hence, the present study addressed the role of MAM in BD by using cell-based models derived from early-stage patients with BD and matched healthy controls.

Results from several microscopy techniques demonstrated increased ER-mitochondria colocalization and higher percentage of close ER-mitochondria contacts (MAM) in BD fibroblasts compared with controls, together with increased levels of the OMM protein VDAC and a qualitative trend towards increased PTPIP51 levels, suggesting alterations in ER-mitochondria tethering in BD. These alterations could be further clarified if the isolation of MAM was feasible in primary fibroblasts since variations in MAM components are more accurately discerned in isolated MAM fractions than total cell extracts (57). To the best of the authors' knowledge, only one previous study has investigated MAM in BD. Based on PLA findings, this study reported a reduction in these contacts in iPSCs-derived neurons from patients with BD compared with controls (58). In the present study, data from PLA analysis were corroborated by other fluorescence microscopy approaches and by TEM analysis, the gold standard technique to measure the distance between these organelles and, thus, to properly evaluate MAM. The discrepancies between the present study and that of Kathuria *et al* (58) might arise from variability in cohorts in terms of age, gender and disease stage, which are determinant factors that can influence outcomes (59). Indeed, this study included only early-stage male patients with BD (BD stage 2) aged between 18-35 years, whereas the previous study included both male and female patients with BD aged between 18-65 years-old, meaning that patients at different disease stages were probably enrolled in the study.

The close ER-mitochondria juxtaposition at MAM facilitates the efficient transfer of both Ca^{2+} and lipids between these organelles. Notably, a decrease of ER-mitochondria Ca^{2+} transfer was observed in BD cells in conditions of MAM upregulation, which might arise from compromised IP3R-mediated ER Ca^{2+} release. The present study data strongly suggested that compromised ER-mitochondria Ca^{2+} transfer in BD fibroblasts was likely to result from the inability of SOCE-mediated extracellular Ca^{2+} influx to replenish ER Ca^{2+} stores, leading to Ca^{2+} depletion that will affect the uptake of Ca^{2+} by mitochondria (49,60). ROS generation in BD cells might be the cause of SOCE impairment, as SOCE is modulated in a redox-dependent manner (61). In agreement, the downregulation of SOCE was recently reported in iPSCs-derived neurons obtained from patients with BD (62). The hypothesis that BD pathophysiology is at least partly caused by aberrant Ca^{2+} homeostasis is supported by alterations in genes encoding to Ca^{2+} channels such as calcium voltage-gated channel subunit α1 C (CACNA1C), identified as greater risk for BD (63).

The similar protein levels of the ER-resident Sigma-1R suggested that the differences between BD and control cells do not arise from alterations in this well-known modulator of the IP3R-mediated ER Ca^{2+} release. However, Sigma-1R activation leading to an antagonistic effect of IP3R in BD fibroblasts cannot be ruled out. Previous reports indicate that Sigma-1R can function in an agonist- or antagonist-sensitive manner, by modulating the interaction between ankyrin B and IP3R3, which in turn affects IP3R-VDAC coupling, thus directly interfering with Ca^{2+} handling (64). Indeed, genetic variations in *SIGMAR1* have been identified in patients with BD (65). Another viable hypothesis is that the deficient transfer of Ca^{2+} between the ER and mitochondria reported in this study may be associated with the mitochondrial dysfunction previously described by our research team in BD fibroblasts (41). Unchanged MCU protein levels ruled out that inhibition of mitochondrial Ca^{2+} uptake at IMM contributes to attenuate the ER-mitochondria Ca^{2+} transfer in BD cells. However, the hypothesis that MCU activity is inhibited in these cells in the absence of changes in protein content cannot be discarded.

To the best of the authors' knowledge, the present study was pioneering in investigating LDs in BD. Its data showing higher number of LDs in BD fibroblasts indicated disrupted lipid metabolism in this pathology, which agrees with previous studies highlighting significant changes in the lipidome of patients with BD (66-69). The increase of LDs in BD cells is expected to arise from heightened lipid transfer at MAM, a crucial place for LDs biogenesis (70). This positive correlation between upregulated MAM and increased LDs content was previously documented in AD (10).

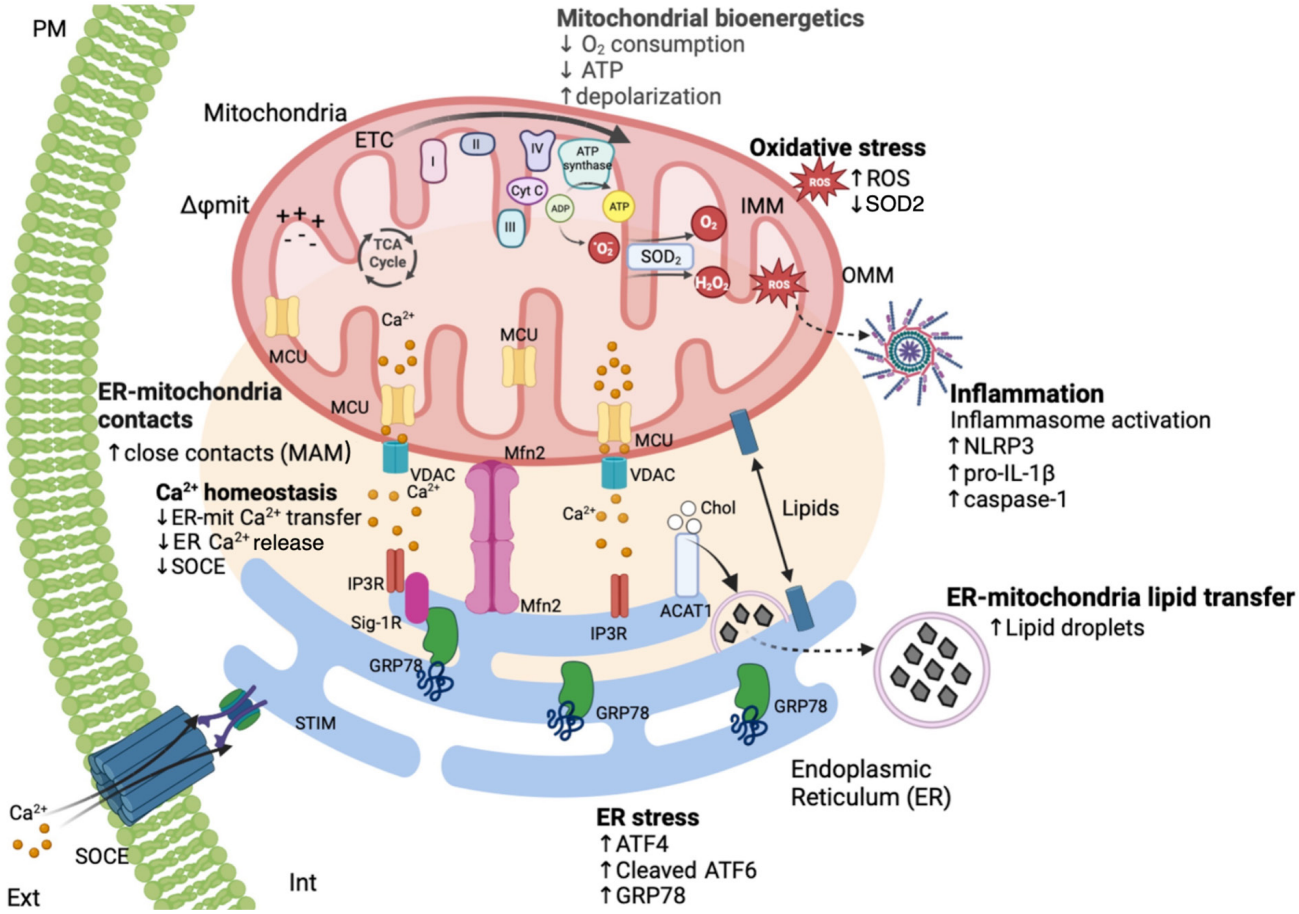

Figure 6. The MAM hypothesis for BD. Fibroblasts derived from patients diagnosed with BD exhibit increased ER-mitochondria apposition and markedly higher percentage of close ER-mitochondria contacts sites (MAM) in comparison with healthy controls, in particular those <20 nm. This structural alteration in the ER-mitochondria juxtaposition directly affects the main functions of MAM, which are the inter-organelle transfer of Ca^{2+} and lipids. As a consequence, ER-mitochondria lipids transfer is enhanced increasing the formation of lipid droplets while Ca^{2+} transfer is inhibited. Concomitantly, BD fibroblasts exhibit lower SOCE and higher oxidative stress levels due to the inhibition of SOD2 mitochondrial antioxidant enzyme and accumulation of ROS in the cytosol and in the mitochondria. In addition to these alterations in Ca^{2+} and redox homeostasis as well as in lipid metabolism, BD-specific changes in MAM are also associated with induction of ER stress and sterile inflammation. A basal pro-inflammatory status in BD is supported by the upregulation of pro-inflammatory cytokines, which seems to be implicated in the diminished susceptibility of both fibroblasts and monocytes derived from patients with BD to inflammatory stimuli, as shown by the lower activation of the NLRP3 inflammasome in response to LPS. PM, plasma membrane; MAM, mitochondria-associated membranes; BD, bipolar disorder; MCU, mitochondrial calcium uniport; Cyt C, cytochrome *c*; TCA cycle, tricarboxylic acid cycle; ADP, adenosine diphosphate; ATP, adenosine triphosphate; O_2, superoxide anion; O_2, oxygen; H_2O_2, hydrogen peroxide; SOD2, superoxide dismutase 2; ROS, reactive oxygen species; VDAC, voltage-dependent anion channels; Mfn2, mitofusin 2; IP3R, inositol trisphosphate receptor; Sig-1R, sigma-1 receptor; ACAT1, Acetyl-CoA acetyltransferase 1; CE, cholesterol ester; SOCE, store-operated calcium entry; STIM1, stromal interaction molecule 1; UPR, unfolded protein response; ER, endoplasmic reticulum; NLRP3, NOD-like receptor family pyrin domain-containing 3; BD, bipolar disorder; LPS, lipopolysaccharide.

LDs have recently emerged as critical players in cellular stress responses (71,72). Disruptions in LDs turnover can instigate ER stress, which in turn can contribute to the accumulation of LDs in several types of cells (73). Accordingly, LDs accumulation in BD fibroblasts coincides with ER stress induction, as demonstrated by increased protein levels of ER stress-induced UPR markers such as ATF4 and ATF6, mediators of PERK and ATF6 UPR branches, respectively, as well as glucose-regulated protein 78 (GRP78), the major ER-resident chaperone. The involvement of ER stress in BD pathophysiology is supported by studies reporting higher GRP78 levels in peripheral blood cells from these patients, as well as by the modulation of this ER stress marker by several mood stabilizers (74,75).

The UPR activation under chronic ER stress conditions markedly enhances the expression of pro-inflammatory cytokines. Specifically, the PERK arm of UPR stimulates IL-6 production, while the ATF-6 branch upregulates IL-1β, IL-6 and TNFα cytokines (76). Notably, the activation of both PERK and ATF6 UPR arms in the fibroblasts of patients with BD occurs concomitantly with increased mRNA levels of pro-IL-1β, TNFα, IL-6 and IL-8. The present study underscored that BD fibroblasts display a baseline pro-inflammatory profile, probably resulting from chronic ER stress. This observation agreed with previous studies consistently reporting a rise of pro-inflammatory cytokines in BD such as TNFα, IL-6 and IL-8 and lower concentrations of anti-inflammatory cytokines, in both manic and depressive BD states (77). Moreover, higher IL-1β levels have been detected in the cerebrospinal fluid of patients with BD, not only during periods of remission following mania but also during euthymic states (78). BD-associated pro-inflammatory status is also further supported by previous findings showing altered numbers of circulating immune cells in peripheral

blood collected from those patients, including monocytes, leukocytes, neutrophils and lymphocytes (42,79,80). Of note, the neuroanatomical white matter brain changes described in patients with BD have been closely linked to immune alterations (81). Additionally, the clinical evidence that these patients exhibit a high prevalence of chronic comorbidities, such as metabolic and autoimmune diseases further strengthens the role of inflammation in BD pathophysiology (82). Evidence from meta-analysis reveals that the incidence of BD is markedly increased in patients with autoimmune diseases such as psoriasis (83). Similarly, psoriasis is often accompanied by psychiatric comorbidities including anxiety and depression, sleep disorders and suicidal behavior (37). This bidirectional interaction highlights the intricate connection between skin diseases and psychiatric conditions, reinforcing the hypothesis of the skin-brain axis in BD. Recently, inflammation has been identified as a key mediator underlying the interaction between psoriasis and mental health commodities. T cells and their secreted inflammatory cytokines play pivotal roles in the pathogenesis of both psoriasis and psychiatric disorders by interacting with the hypothalamic-pituitary-adrenal axis, exacerbating immune dysregulation and disease progression (37). Notably, a basal pro-inflammatory status is evident in patients with BD, as shown by elevated levels of pro-inflammatory cytokines in fibroblasts derived from them. This inflammatory profile observed in fibroblasts from patients with BD might suggest that dysregulated immune responses and chronic inflammation are key players in disease development. Moreover, these findings may reflect the neuroinflammatory environment described in the brains of patients with BD (84), further supporting the skin-brain axis as a critical route for understanding this complex neuropsychiatric condition.

The activation of both IRE1a and PERK UPR pathways induces the expression of pro-IL-1β and NLRP3 via NF-kB, promoting the NLRP3 inflammasome activation and subsequent IL-1β release (85). Notably, mitochondrial ROS, which were found increased in BD fibroblasts, primarily due to the inhibition of SOD2 mitochondrial antioxidant enzyme, have been recognized as classical triggers for NLRP3 inflammasome activation (14). In agreement, oxidative stress has been implicated in BD pathophysiology (86). Furthermore, variations in genes encoding antioxidant enzymes such as SOD2 and glutathione peroxidase 3 have been reported in patients with BD (87). For instance, the polymorphism rs4880 in SOD2, identified as a BD risk factor, results in reduced activity of this enzyme (88).

Notably, NLRP3 inflammasome assembly takes place at MAM platforms (13). Therefore, the upregulation of MAM in fibroblasts from patients with BD can be responsible for NLRP3 inflammasome activation, as evidenced by increased mRNA levels of NLRP3 and pro-IL-1β, along with enhanced caspase-1 activity, compared with controls. The pivotal role of NLRP3 inflammasome in fostering the BD-associated pro-inflammatory state has already been suggested by the upregulation of IL-1β, NLRP3, ASC and caspase-1 in post-mortem frontal cortex of patients with BD (26). The present study disclosed that NLRP3 inflammasome activation under LPS-induced inflammation-prone conditions was markedly lower in BD cells compared with controls. Although fibroblasts possess the capability to modulate inflammatory responses, their cytokines secretion is relatively modest compared with immune cells (89,90), therefore, this study also explored NLRP3 inflammasome activation in LPS-treated primary monocytes isolated from both patients with BD and controls, and similar results were obtained. Together, the present study suggested a diminished responsiveness of cells from patients with BD to inflammation-prone stressful conditions. The lower resilience exhibited by BD cells can be attributed to the pre-activated state of NLRP3 inflammasome under non-stimulated conditions. This hypothesis is strengthened by our previous findings, showing that NLRP3 inflammasome activation occurs in BD monocytes upon ER stress induction, even in the absence of LPS priming (42). Accordingly, ATP treatment in fibroblasts from patients with systemic sclerosis, which are in pre-activated state, also induces IL-6 release in the absence of LPS priming (91). Lastly, the reduced cellular resilience due to compromised NLRP3 inflammasome activity in BD may contribute to explain the high prevalence of infectious diseases in these patients (92).

Fibroblasts and blood cells from individuals with diagnosis of multiple brain diseases, including neuropsychiatric conditions such as BD, have long been considered as valuable patient-derived cell models, markedly contributing to increasing our knowledge about the pathophysiology of brain disorders. Although the findings of this study obtained in fibroblasts and monocytes derived from patients with BD and control individuals corroborate its conclusions, some limitations have been identified: i) the sample size was relatively small; however, the statistically significant differences observed between control and BD cells support the present study as a pioneering proof-of-concept demonstration of the role of MAM in BD; ii) the present study focused exclusively on early-stage patients with BD and did not include an assessment of later-stage cases, which should be addressed in future studies; and iii) validation using neurons differentiated from iPSCs could further strengthen the evidence of MAM impairment in BD.

The comprehensive structural and functional analysis conducted on cells obtained from early-stage patients with BD and healthy controls markedly contributes to unravelling the pivotal role of MAM in BD pathophysiology (Fig. 6). The increased ER-mitochondria juxtaposition at MAM observed in BD cells correlated with enhanced lipid transfer and formation of LDs, which occurs concomitantly with decreased ER-mitochondria Ca^{2+} transfer that is associated with impaired SOCE activity and a subsequent inability to refill ER Ca^{2+} stores. The dysfunction of MAM may underlie the previously reported mitochondrial respiratory impairment and ATP depletion in BD cells (41), as well as the induction of MAM-associated events identified in the present study, including oxidative stress, ER stress-induced UPR and basal NLRP3 inflammasome activation.

Although further research is needed, the present study suggested that the skin-brain axis may provide a novel route for understanding the pathophysiology of BD, with inflammation potentially being a central mediator between these interconnected systems.

In conclusion, MAM impairment was underscored as a key pathophysiological mechanism in early BD stages suggesting

that these subcellular structures should be further exploring to search novel therapeutic targets.

Acknowledgements

Not applicable.

Funding

The present study was supported by the European Regional Development Fund (ERDF), through the Centro 2020 Regional Operational Programme under grant no. CENTRO-01-0145-FEDER-000012 (HealthyAging2020) and through the COMPETE 2020-Operational Programme for Competitiveness and Internationalization and Portuguese national funds via FCT-Fundação para a Ciência e a Tecnologia, under grant nos. PTDC/MED-NEU/28214/2017, PTDC/MED-FAR/29369/2017 and UIDB/04539/2020, UIDP/04539/2020 and LA/P/0058/2020. AP is a PhD fellow from FCT (grant no. SFRH/BD/148653/2019). RR is Post-Doctoral Researcher (grant no. DL 57/2016/CP1448/CT0012).

Availability of data and materials

The data generated in the present study are included in the figures and/or tables of this article.

Authors' contributions

ACP: Data curation, formal analysis, investigation, writing-original draft. APM, RR, MC, TF, LSC: Data curation, formal analysis, investigation. MB, JBDM, AM: Resources, methodology. NM: Resources, methodology, funding acquisition. CC, MTC: Supervision, writing-review and editing. CFP: Conceptualization, supervision, project administration, funding acquisition, writing-review and editing. All authors read and approved the final manuscript.

Ethics approval and consent to participate

The study was approved by the Ethics Committee of the Centro Hospitalar e Universitário de Coimbra (now ULS de Coimbra), reference 150/CES, July 3, 2018 and both the skin biopsies and the peripheral blood samples were taken following informed consent also approved by the same ethics committee (30).

Patient consent for publication

Not applicable.

Competing interests

The authors declare that they have no competing interests.

References

1. Csordás G, Renken C, Várnai P, Walter L, Weaver D, Buttle KF, Balla T, Mannella CA and Hajnóczky G: Structural and functional features and significance of the physical linkage between ER and mitochondria. J Cell Biol 174: 915-921, 2006.
2. Filadi R, Theurey P and Pizzo P: The endoplasmic reticulum-mitochondria coupling in health and disease: Molecules, functions and significance. Cell Calcium 62: 1-15, 2017.
3. Wang X, Wen Y, Dong J, Cao C and Yuan S: Systematic In-depth proteomic analysis of Mitochondria-associated endoplasmic reticulum membranes in mouse and human testes. Proteomics 18: e1700478, 2018.
4. Rowland AA and Voeltz GK: Endoplasmic reticulum-mitochondria contacts: Function of the junction. Nat Rev Mol Cell Biol 13: 607-625, 2012.
5. de Brito OM and Scorrano L: Mitofusin-2 regulates mitochondrial and endoplasmic reticulum morphology and tethering: The role of Ras. Mitochondrion 9: 222-226, 2009.
6. Casellas-D Iaz S, Larramona-Arcas R, Riqu E-Pujol G, Tena-Morraja P, Müller-Sánchez C, Segarra-Mondejar M, Gavaldà-Navarro A, Villarroya F, Reina M, Martínez-Estrada OM and Soriano FX: Mfn2 localization in the ER is necessary for its bioenergetic function and neuritic development. EMBO Rep 22: e51954, 2021.
7. Yang S, Zhou R, Zhang C, He S and Su Z: Mitochondria-associated endoplasmic reticulum membranes in the pathogenesis of type 2 diabetes mellitus. Front Cell Dev Biol 8: 571554, 2020.
8. Gómez-Suaga P, Pérez-Nievas BG, Glennon EB, Lau DHW, Paillusson S, Mórotz GM, Calì T, Pizzo P, Noble W and Miller CCJ: The VAPB-PTPIP51 endoplasmic reticulum-mitochondria tethering proteins are present in neuronal synapses and regulate synaptic activity. Acta Neuropathol Commun 7: 35, 2019.
9. Xu H, Guan N, Ren YL, Wei QJ, Tao YH, Yang GS, Liu XY, Bu DF, Zhang Y and Zhu SN: IP3R-Grp75-VDAC1-MCU calcium regulation axis antagonists protect podocytes from apoptosis and decrease proteinuria in an Adriamycin nephropathy rat model. BMC Nephrol 19: 140, 2018.
10. Area-Gomez E, Del Carmen Lara Castillo M, Tambini MD, Guardia-Laguarta C, de Groof AJ, Madra M, Ikenouchi J, Umeda M, Bird TD, Sturley SL and Schon EA: Upregulated function of mitochondria-associated ER membranes in Alzheimer disease. EMBO J 31: 4106-4123, 2012.
11. Raturi A and Simmen T: Where the endoplasmic reticulum and the mitochondrion tie the knot: The mitochondria-associated membrane (MAM). Biochimica et Biophysica Acta (BBA)-Mol Cell Res 1833: 213-224, 2013.
12. van Vliet AR, Verfaillie T and Agostinis P: New functions of mitochondria associated membranes in cellular signaling. Biochim Biophys Acta 1843: 2253-2262, 2014.
13. Zhou R, Yazdi AS, Menu P and Tschopp J: A role for mitochondria in NLRP3 inflammasome activation. Nature 469: 221-225, 2011.
14. Kelley N, Jeltema D, Duan Y and He Y: The NLRP3 inflammasome: An overview of mechanisms of activation and regulation. Int J Mol Sci 20: 3328, 2019.
15. Missiroli S, Patergnani S, Caroccia N, Pedriali G, Perrone M, Previati M, Wieckowski MR and Giorgi C: Mitochondria-associated membranes (MAMs) and inflammation. Cell Death Dis 9: 329, 2018.
16. Filadi R, Greotti E and Pizzo P: Highlighting the endoplasmic reticulum-mitochondria connection: Focus on Mitofusin 2. Pharmacol Res 128: 42-51, 2018.
17. Area-Gomez E, de Groof A, Bonilla E, Montesinos J, Tanji K, Boldogh I, Pon L and Schon EA: A key role for MAM in mediating mitochondrial dysfunction in Alzheimer disease. Cell Death Dis 9: 335, 2018.
18. Resende R, Fernandes T, Pereira AC, Marques AP and Pereira CF: Endoplasmic Reticulum-mitochondria contacts modulate reactive oxygen Species-mediated signaling and oxidative stress in brain disorders: The key role of Sigma-1 receptor. Antioxid Redox Signal 37: 758-780, 2022.
19. Elsayed OH, Ercis M, Pahwa M and Singh B: Treatment-resistant bipolar depression: Therapeutic trends, challenges and future directions. Neuropsychiatr Dis Treat 18: 2927-2943, 2022.
20. Huang Y, Zhang Z, Lin S, Zhou H and Xu G: Cognitive impairment mechanism in patients with bipolar disorder. Neuropsychiatr Dis Treat 19: 361-366, 2023.
21. Sampogna G, Janiri D, Albert U, Caraci F, Martinotti G, Serafini G, Tortorella A, Zuddas A, Sani G and Fiorillo A: Why lithium should be used in patients with bipolar disorder? A scoping review and an expert opinion paper. Expert Rev Neurother 22: 923-934, 2022.
22. Hu X, Yu C, Dong T, Yang Z, Fang Y and Jiang Z: Biomarkers and detection methods of bipolar disorder. Biosens Bioelectron 220: 114842, 2023.

23. Pereira AC, Resende R, Morais S, Madeira N and Fragão Pereira C: The ups and downs of cellular stress: The 'MAM hypothesis' for Bipolar disorder pathophysiology. International J Clin Neurosciences Mental Health: S04, 2017.
24. Pereira AC, Oliveira J, Silva S, Madeira N, Pereira CMF and Cruz MT: Inflammation in bipolar disorder (BD): Identification of new therapeutic targets. Pharmacol Res 163: 105325, 2021.
25. Resende R, Fernandes T, Pereira AC, De Pascale J, Marques AP, Oliveira P, Morais S, Santos V, Madeira N, Pereira CF and Moreira PI: Mitochondria, endoplasmic reticulum and innate immune dysfunction in mood disorders: Do Mitochondria-associated Membranes (MAMs) play a role? Biochim Biophys Acta Mol Basis Dis 1866: 165752, 2020.
26. Kim HK, Andreazza AC, Elmi N, Chen W and Young LT: Nod-like receptor pyrin containing 3 (NLRP3) in the post-mortem frontal cortex from patients with bipolar disorder: A potential mediator between mitochondria and immune-activation. J Psychiatr Res 72: 43-50, 2016.
27. Viswanath B, Jose SP, Squassina A, Thirthalli J, Purushottam M, Mukherjee O, Vladimirov V, Patrinos GP, Del Zompo M and Jain S: Cellular models to study bipolar disorder: A systematic review. J Affect Disord 184: 36-50, 2015.
28. Johnston JA, Cowburn RF, Norgren S, Wiehager B, Venizelos N, Winblad B, Vigo-Pelfrey C, Schenk D, Lannfelt L and O'Neill C: Increased β-amyloid release and levels of amyloid precursor protein (APP) in fibroblast cell lines from family members with the Swedish Alzheimer's disease APP670/671 mutation. FEBS Lett 354: 274-278, 1994.
29. Hoepken HH, Gispert S, Azizov M, Klinkenberg M, Ricciardi F, Kurz A, Morales-Gordo B, Bonin M, Riess O, Gasser T, *et al*: Parkinson patient fibroblasts show increased alpha-synuclein expression. Exp Neurol 212: 307-313, 2008.
30. Onofre I, Mendonça N, Lopes S, Nobre R, de Melo JB, Carreira IM, Januário C, Gonçalves AF and de Almeida LP: Fibroblasts of machado joseph disease patients reveal autophagy impairment. Sci Rep 6: 28220, 2016.
31. Oliveira NC, Russo FB and Beltrão-Braga PCB: Differentiation of peripheral sensory neurons from iPSCs derived from stem cells from human exfoliated deciduous teeth (SHED). Front Cell Dev Biol 11: 1203503, 2023.
32. Kálmán S, Garbett KA, Janka Z and Mirnics K: Human dermal fibroblasts in psychiatry research. Neuroscience 320: 105-121, 2016.
33. Etemadikhah M, Niazi A, Wetterberg L and Feuk L: Transcriptome analysis of fibroblasts from schizophrenia patients reveals differential expression of schizophrenia-related genes. Sci Rep 10: 630, 2020.
34. Akin D, Manier DH, Sanders-Bush E and Shelton RC: Decreased serotonin 5-HT2A receptor-stimulated phosphoinositide signalling in fibroblasts from melancholic deppresed patients. Neuropsychopharmacology 29: 2081-2087, 2004.
35. Jameson C, Boulton KA, Silove N, Nanan R and Guastella AJ: Ectodermal origins of the skin-brain axis: A novel model for the developing brain, inflammation, and neurodevelopmental conditions. Mol Psychiatry 28: 108-117, 2023.
36. Kim HS, Jung H, Park YH, Heo SH, Kim S and Moon M: Skin-brain axis in Alzheimer's disease-Pathologic, diagnostic, and therapeutic implications: A hypothetical review. Aging Dis 16: 901-916, 2024.
37. Yang J, Zhang S, Wu Q, Chen P, Dai Y, Long J, Wu Y and Lin Y: T cell-mediated skin-brain axis: Bridging the gap between psoriasis and psychiatric comorbidities. J Autoimmun 144: 103176, 2024.
38. Berk M, Post R, Ratheesh A, Gliddon E, Singh A, Vieta E, Carvalho AF, Ashton MM, Berk L, Cotton SM, *et al*: Staging in bipolar disorder: From theoretical framework to clinical utility. World Psychiatry 16: 236-244, 2017.
39. American Psychiatric Association: Diagnostic and Statistical Manual of Mental Disorders. Diagnostic and Statistical Manual of Mental Disorders, 2013.
40. Martins MJ, Palmeira L, Xavier A, Castilho P, Macedo A, Pereira AT, Pinto AM, Carreiras D and Barreto-Carvalho C: The clinical interview for psychotic disorders (CIPD): Preliminary results on interrater agreement, reliability and qualitative feedback. Psychiatry Res 272: 723-729, 2019.
41. Marques AP, Resende R, Silva DF, Batista M, Pereira D, Wildenberg B, Morais S, Macedo A, Pais C, Melo JB, *et al*: Mitochondrial alterations in fibroblasts of early stage bipolar disorder patients. Biomedicines 9: 522, 2021.
42. Pereira AC, De Pascale J, Resende R, Cardoso S, Ferreira I, Neves BM, Carrascal MA, Zuzarte M, Madeira N, Morais S, *et al*: ER-mitochondria communication is involved in NLRP3 inflammasome activation under stress conditions in the innate immune system. Cell Mol Life Sci 79: 213, 2022.
43. Pereira AC, Madeira N, Morais S, Macedo A, Cruz MT and Pereira CMF: Mitochondria fusion upon SERCA inhibition prevents activation of the NLRP3 inflammasome in human monocytes. Cells 11: 433, 2022.
44. Bolte S and Cordelières FP: A guided tour into subcellular colocalization analysis in light microscopy. J Microsc 224: 213-232, 2006.
45. Tiscione SA, Vivas O, Ginsburg KS, Bers DM, Ory DS, Santana LF, Dixon RE and Dickson EJ: Disease-associated mutations in Niemann-Pick type C1 alter ER calcium signaling and neuronal plasticity. J Cell Biol 218: 4141-4156, 2019.
46. Moreira P, Sousa FJ, Matos P, Brites GS, Gonçalves MJ, Cavaleiro C, Figueirinha A, Salgueiro L, Batista MT, Branco PC, *et al*: Chemical composition and effect against skin alterations of bioactive extracts obtained by the hydrodistillation of eucalyptus globulus leaves. Pharmaceutics 14: 561, 2022.
47. Livak KJ and Schmittgen TD: Analysis of relative gene expression data using real-time quantitative PCR and the 2(-Delta Delta C(T)) method. Methods 25: 402-408, 2001.
48. Hayashi A, Kasahara T, Kametani M, Toyota T, Yoshikawa T and Kato T: Aberrant endoplasmic reticulum stress response in lymphoblastoid cells from patients with bipolar disorder. Int J Neuropsychopharmacol 12: 33-43, 2009.
49. Seegren PV, Harper LR, Downs TK, Zhao XY, Viswanathan SB, Stremska ME, Olson RJ, Kennedy J, Ewald SE, Kumar P and Desai BN: Reduced mitochondrial calcium uptake in macrophages is a major driver of inflammaging. Nat Aging 3: 796-812, 2023.
50. Nan J, Li J, Lin Y, Saif Ur Rahman M, Li Z and Zhu L: The interplay between mitochondria and store-operated Ca2+ entry: Emerging insights into cardiac diseases. J Cell Mol Med 25: 9496-9512, 2021.
51. Zhao J, Li J, Li G and Chen M: The role of mitochondria-associated membranes mediated ROS on NLRP3 inflammasome in cardiovascular diseases. Front Cardiovasc Med 9: 1059576, 2022.
52. van Vliet AR and Agostinis P: Mitochondria-associated membranes and ER stress. Curr Top Microbiol Immunol 414: 73-102, 2018.
53. Guo H, Callaway JB and Ting JPY: Inflammasomes: Mechanism of action, role in disease, and therapeutics. Nat Med 21: 677-687, 2015.
54. Walsh JG, Muruve DA and Power C: Inflammasomes in the CNS. Nat Rev Neurosci 15: 84-97, 2014.
55. He Y, Hara H and Núñez G: Mechanism and regulation of NLRP3 inflammasome activation. Trends Biochem Sci 41: 1012-1021, 2016.
56. Davidson S, Coles M, Thomas T, Kollias G, Ludewig B, Turley S, Brenner M and Buckley CD: Fibroblasts as immune regulators in infection, inflammation and cancer. Nat Rev Immunol 21: 704-717, 2021.
57. Fernandes T, Resende R, Silva DF, Marques AP, Santos AE, Cardoso SM, Domingues MR, Moreira PI and Pereira CF: Structural and functional alterations in mitochondria-associated membranes (MAMs) and in mitochondria activate stress response mechanisms in an in vitro model of Alzheimer's disease. Biomedicines 9: 881, 2021.
58. Kathuria A, Lopez-Lengowski K, Vater M, McPhie D, Cohen BM and Karmacharya R: Transcriptome analysis and functional characterization of cerebral organoids in bipolar disorder. Genome Med 12: 34, 2020.
59. Rich-Edwards JW, Kaiser UB, Chen GL, Manson JAE and Goldstein JM: Sex and gender differences research design for basic, clinical, and population studies: Essentials for investigators. Endocr Rev 39: 424-439, 2018.
60. Trebak M and Putney JW Jr: ORAI Calcium channels. Physiology 32: 332-342, 2017.
61. Nunes P and Demaurex N: Redox regulation of store-operated Ca2+ entry. Antioxid Redox Signal 21: 915-932, 2014.
62. Hewitt T, Alural B, Tilak M, Wang J, Becke N, Chartley E, Perreault M, Haggarty SJ, Sheridan SD, Perlis RH, *et al*: Bipolar disorder-iPSC derived neural progenitor cells exhibit dysregulation of store-operated Ca2+ entry and accelerated differentiation. Mol Psychiatry 28: 5237-5250, 2023.
63. Nurnberger JI Jr, Koller DL, Jung J, Edenberg HJ, Foroud T, Guella I, Vawter MP and Kelsoe JR; Psychiatric Genomics Consortium Bipolar Group: Identification of pathways for bipolar disorder: A meta-analysis. JAMA Psychiatry 71: 657-664, 2014.

64. Weng TY, Tsai SYA and Su TP: Roles of sigma-1 receptors on mitochondrial functions relevant to neurodegenerative diseases. J Biomed Sci 24: 74, 2017.
65. Mandelli L, Wang SM, Han C, Lee SJ, Patkar AA, Masand PS, Pae CU and Serretti A: The impact of a single nucleotide polymorphism in SIGMAR1 on depressive symptoms in major depressive disorder and bipolar disorder. Adv Ther 34: 713-724, 2017.
66. Scola G, Versace A, Metherel AH, Monsalve-Castro LA, Phillips ML, Bazinet RP and Andreazza AC: Alterations in peripheral fatty acid composition in bipolar and unipolar depression. J Affect Disord 233: 86-91, 2018.
67. Knowles EEM, Meikle PJ, Huynh K, Göring HH, Olvera RL, Mathias SR, Duggirala R, Almasy L, Blangero J, Curran JE and Glahn DC: Serum phosphatidylinositol as a biomarker for bipolar disorder liability. Bipolar Disord 19: 107-115, 2017.
68. Ribeiro HC, Klassen A, Pedrini M, Carvalho MS, Rizzo LB, Noto MN, Zeni-Graiff M, Sethi S, Fonseca FAH, Tasic L, *et al*: A preliminary study of bipolar disorder type I by mass spectrometry-based serum lipidomics. Psychiatry Res 258: 268-273, 2017.
69. Guo L, Zhang T, Li R, Cui ZQ, Du J, Yang JB, Xue F, Chen YH, Tan QR and Peng ZW: Alterations in the plasma lipidome of adult women with bipolar disorder: A mass spectrometry-based lipidomics research. Front Psychiatry 13: 802710, 2022.
70. Zhu Y, Chen CY, Li J, Cheng JX, Jang M and Kim KH: In vitro exploration of ACAT contributions to lipid droplet formation during adipogenesis. J Lipid Res 59: 820-829, 2018.
71. Henne WM, Reese ML and Goodman JM: The assembly of lipid droplets and their roles in challenged cells. EMBO J 37: e98947, 2018.
72. Olzmann JA and Carvalho P: Dynamics and functions of lipid droplets. Nat Rev Mol Cell Biol 20: 137-155, 2019.
73. Jarc E and Petan T: Lipid droplets and the management of cellular stress. Yale J Biol Med 92: 435-452, 2019.
74. Bengesser SA, Fuchs R, Lackner N, Birner A, Reininghaus B, Meier-Allard N, Stracke A, Kapfhammer HP, Reininghaus EZ and Wallner-Liebmann S: Endoplasmic reticulum stress and bipolar disorder-Almost forgotten therapeutic drug targets in the unfolded protein response pathway revisited. CNS Neurol Disord Drug Targets 15: 403-413, 2016.
75. Bengesser SA, Reininghaus EZ, Dalkner N, Birner A, Hohenberger H, Queissner R, Fellendorf F, Platzer M, Pilz R, Hamm C, *et al*: Endoplasmic reticulum stress in bipolar disorder? -BiP and CHOP gene expression- and XBP1 splicing analysis in peripheral blood. Psychoneuroendocrinology 95: 13-119, 2018.
76. Thoudam T, Jeon JH, Ha CM and Lee IK: Role of mitochondria-associated endoplasmic reticulum membrane in inflammation-mediated metabolic diseases. Mediators Inflamm 2016: 1851420, 2016.
77. Sayana P, Colpo GD, Simões LR, Giridharan VV, Teixeira AL, Quevedo J and Barichello T: A systemic review of evidence for the role of inflammatory biomarkers in bipolar patients. J Psychiatr Res 92: 160-182, 2017.
78. Söderlund J, Olsson S, Samuelsson M, Walther-Jallow L, Johansson C, Erhardt S, Landén M and Engberg G: Elevation of cerebrospinal fluid interleukin-1β in bipolar disorder. J Psychiatry Neurosci 36: 114-118, 2011.
79. Munkholm K, Jacoby AS, Lenskjold T, Bruunsgaard H, Vinberg M and Kessing LV: Leukocytes in peripheral blood in patients with bipolar disorder-Trait and state alterations and association with levels of cytokines and C-reactive protein. Psychiatry Res 261: 383-390, 2018.
80. Barbosa IG, Rocha NP, Assis F, Vieira ELM, Soares JC, Bauer ME and Teixeira AL: Monocyte and lymphocyte activation in bipolar disorder: A new piece in the puzzle of immune dysfunction in mood disorders. Int J Neuropsychopharmacol 18: pyu021, 2014.
81. Magioncalda P, Martino M, Tardito S, Sterlini B, Conio B, Marozzi V, Adavastro G, Capobianco L, Russo D, Parodi A, *et al*: White matter microstructure alterations correlate with terminally differentiated CD8+ effector T cell depletion in the peripheral blood in mania: Combined DTI and immunological investigation in the different phases of bipolar disorder. Brain Behav Immun 73: 192-204, 2018.
82. SayuriYamagata A, Brietzke E, Rosenblat JD, Kakar R and McIntyre RS: Medical comorbidity in bipolar disorder: The link with metabolic-inflammatory systems. J Affect Disord 211: 99-106, 2017.
83. Chen M, Jiang Q and Zhang L: The prevalence of bipolar disorder in autoimmune disease: A systematic review and meta-analysis. Ann Palliat Med 10: 350-361, 2021.
84. Lima DD, Cyrino LAR, Ferreira GK, Magro DDD, Calegari CR, Cabral H, Cavichioli N, Ramos SA, Ullmann OM, Mayer Y, *et al*: Neuroinflammation and neuroprogression produced by oxidative stress in euthymic bipolar patients with different onset disease times. Sci Rep 12: 16742, 2022.
85. Zhou Y, Tong Z, Jiang S, Zheng W, Zhao J and Zhou X: The roles of endoplasmic reticulum in NLRP3 inflammasome activation. Cells 9: 1219, 2020.
86. Kotzaeroglou A and Tsamesidis I: The role of equilibrium between free radicals and antioxidants in depression and bipolar disorder. Medicines (Basel) 9: 57, 2022.
87. Zou Y, Kennedy KG, Grigorian A, Fiksenbaum L, Freeman N, Zai CC, Kennedy JL, MacIntosh BJ and Goldstein BI: Antioxidative defense genes and brain structure in youth bipolar disorder. Int J Neuropsychopharmacol 25: 89-98, 2022.
88. Gallegos-Arreola MP, Ramírez-Patiño R, Sánchez-López JY, Zúñiga-González GM, Figuera LE, Delgado-Saucedo JI, Gómez-Meda BC, Rosales-Reynoso MA, Puebla-Pérez AM, Lemus-Varela ML, *et al*: SOD2 Gene Variants (rs4880 and rs5746136) and Their Association with Breast Cancer Risk. Curr Issues Mol Biol 44: 5221-5233, 2022.
89. van Linthout S, Miteva K and Tschöpe C: Crosstalk between fibroblasts and inflammatory cells. Cardiovasc Res 102: 258-269, 2014.
90. Sandanger Ø, Ranheim T, Vinge LE, Bliksøen M, Alfsnes K, Finsen AV, Dahl CP, Askevold ET, Florholmen G, Christensen G, *et al*: The NLRP3 inflammasome is up-regulated in cardiac fibroblasts and mediates myocardial ischaemia-reperfusion injury. Cardiovasc Res 99: 164-174, 2013.
91. lo Monaco A, Gulinelli S, Castellino G, Solini A, Ferrari D, La Corte R, Trotta F and Di Virgilio F: Increased sensitivity to extracellular ATP of fibroblasts from patients affected by systemic sclerosis. Ann Rheum Dis 66: 1124-1125, 2007.
92. Rosenblat JD and McIntyre RS: Bipolar disorder and immune dysfunction: Epidemiological findings, proposed pathophysiology and clinical implications. Brain Sci 7: 144, 2017.